2017

Fluorescence Polarization Measurements To Probe Alignment Of A Bithiophene Dye In One-Dimensional Channels Of Self-Assembled Phenylethynylene Bis-Urea Macrocycle Crystals

Preecha Kittikhunnatham
University of South Carolina

FLUORESCENCE POLARIZATION MEASUREMENTS TO PROBE ALIGNMENT OF A BITHIOPHENE DYE IN ONE-DIMENSIONAL CHANNELS OF SELF-ASSEMBLED PHENYLETHYNYLENE BIS-UREA MACROCYCLE CRYSTALS

by

Preecha Kittikhunnatham

Bachelor of Science
Chulalongkorn University, 2012

Submitted in Partial Fulfillment of the Requirements

For the Degree of Master of Science in

Chemistry

College of Arts and Sciences

University of South Carolina

2017

Accepted by:

Andrew B. Greytak, Director of Thesis

Linda S. Shimizu, Reader

Cheryl L. Addy, Vice Provost and Dean of the Graduate School

DEDICATION

This thesis is dedicated to my parents, Somphong Kittikhunnatham and Choei Pruethong, and my sister, Pornpan Kittikhunnatham.

ACKNOWLEDGEMENTS

I would like to thank to my advisor, Dr. Andrew B. Greytak, for his guidance and supports, which help me achieve a successful graduate student path. In addition, I would like to thank all of my research collaborators including, Bozumeh Som, Dr. Vitaly Rassolov, Dr. Matthias Stolte, Dr. Frank Würthner, Dr. Linda S. Shimizu, and Dr. Andrew B. Greytak, to help me complete the study described in this thesis. Moreover, the study described in this thesis made use of the South Carolina SAXS Collaborative and the computer cluster located at department of Chemistry and Biochemistry, University of South Carolina. Finally, I would like to acknowledge a Development and Promotion of Science and Technology Talents Project graduate fellowship from the Royal Government of Thailand for financial support throughout my graduate study.

ABSTRACT

This thesis describes the use of polarized fluorescence microscopy to directly probe guest molecule orientation in bis-urea macrocycle crystals. These macrocycles assemble to afford one-dimensional (1D) microchannels ~9 Å in diameter that have previously been shown to exhibit normal Fickian diffusion and induce selective reactivity among the confined guest molecules. In the present work, we take advantage of the quasi-1D morphology of fiber-like microcrystals with the extended dimension corresponding to the channel axis to measure excitation and emission polarization values for a bithiophene guest. Guest fluorescence is shown to be polarized along the fiber axis with emission polarization values up to 0.729, indicating a high degree of orientational order within the 1D channels. The observed behavior is consistent with calculated results for the guest orientation and electronic transition dipole moment. The results indicate the value of functional fluorescent probes as a measure of guest confinement in low-dimensional environments.

TABLE OF CONTENTS

LIST OF FIGURES

CHAPTER 1

INTRODUCTION[1]

Crystalline materials with simple one-dimensional (1D) channels provide excellent model systems for studying complex processes, including adsorption, diffusion, and molecular recognition and for probing the effects of confinement on the encapsulated guest's electronic properties and reactivity.[1-3] A wide variety of porous solids have been reported with 1D channels that can uptake solvents, gases, and guests. Such solids include porous zeolites,[4-8] tris(*o*-phenylenedioxy)cyclotriphosphazene (TPP),[9, 10] and perhydrotriphenylene (PHTP)[11, 12] inclusion complexes. Organization, especially orientation, of the guest molecules in 1D channels is a crucial factor influencing chemical reactivity, birefringence, energy transfer, and electron transfer among guests. An improved understanding of guest orientation and diffusion[13] in 1D channels is also of interest for the development of chemical sensors[14] and organic electronics.[15]

Macrocycle **1** is composed of C-shaped phenylethynylene spacers linking two urea motifs and self-assembles by slow cooling from DMSO to give fiber-like single crystals **2**.[1] X-ray diffraction demonstrates that the macrocycles are stacked in a columnar fashion, each column enclosing a 1D channel. After activation by removal of the included DMSO

[1] Kittikhunnatham, P.; Som, B.; Rassolov, V.; Stolte, M.; Würthner, F.; Shimizu, L. S.; Greytak A. B. Fluorescence polarization measurements to probe alignment of a bithiophene dye in one-dimensional channels of self-assembled phenylethynylene bis-urea macrocycle crystals. *J. Phys. Chem. C* **2017**, *121* (33), 18102–18109. Reprinted here with permission of publisher.

solvent, the channels can be used as a container for stereoselective photodimerization of encapsulated guests such as coumarin, chromone, and acenaphthalene.[2,16] The channels in the activated fibers have a round cross section with a diameter of ~9.0 Å and are amenable to molecular transport studies on micrometer scales, for example, revealing Fickian diffusion dynamics using hyperpolarized ^{129}Xe NMR.[13] Larger molecules can be expected to experience stronger interactions with the host and constraints on diffusion.

Herein, we investigate the uptake and orientation of a fluorescent push–pull dye within the columnar channels of **2** (Figure 1). The small and elongated dye 5-(dimethylamino)-5′-nitro-2,2′-bithiophene **3**[17, 18] has a strong ground state dipole moment (7.95 D), pronounced solvatochromism, and favorable molecular dimensions (11.7 × 3.5 Å) for intercalation into the channels of **2**. This dye has also been studied in liquid crystals[19] and in films as optic and electrochemical sensors.[20] We employed polarimetric fluorescence microscopy, a technique that has previously been applied to fluorophores in cocrystallized organic inclusion complexes,[21] coupled with image analysis to probe the orientation of **3** within in host–guest fibers **4**. The needle- or fiber-like shape of the crystals permits assignment of the 1D fiber axis. In addition, density functional theory (DFT) was used to predict the orientation of the guest molecules in the 1D channels, and a time-dependent DFT (TDDFT) calculation was used to confirm the orientation of the lowest-energy electronic transition dipole in the guest. The experiments reveal a close correspondence between the long axis of the macrocycle fibers and the linear transition dipole orientation of the guest, as determined from excitation and emission polarization anisotropy measurements of the host–guest complex crystal fibers. We compare these results to the orientation of the guests obtained from the calculations. The determination of

guest orientation in a channel of self-assembled bis-urea macrocycle fibers could aid in optimizing reactions, energy transfer, and electron transfer among guest species.

In lieu of single crystal diffraction data, it can be challenging to establish the orientation of guest molecules within 1D channels, although computational methods[22-26] and dielectric spectroscopy[27] have been applied. An alternative approach that can be applied to fluorescent guests is polarimetric fluorescence imaging, as the apparent fluorescence intensity of guest molecules with linearly or plane polarized transition dipoles varies depending on the orientation of these dipoles with respect to the polarization of the excitation light and/or emission filter. Indeed, fluorescent host–guest complex materials can display high polarization anisotropy as was reported for guests in organic hosts,[21, 28-30] inorganic hosts,[31-34] and biological complexes.[35] Salient features of the polarimetric approach are its sensitivity and high spatial resolution, which provide information for host–guest complexes even for small single crystals. In addition, this technique can be applied over a large range of guest loading factors. Such analysis is particularly well-suited to crystals with quasi-1D shapes, such as semiconductor nanowires[36] and the microcrystals studied here because of the possibility of averaging signals along the 1D axis.[3]

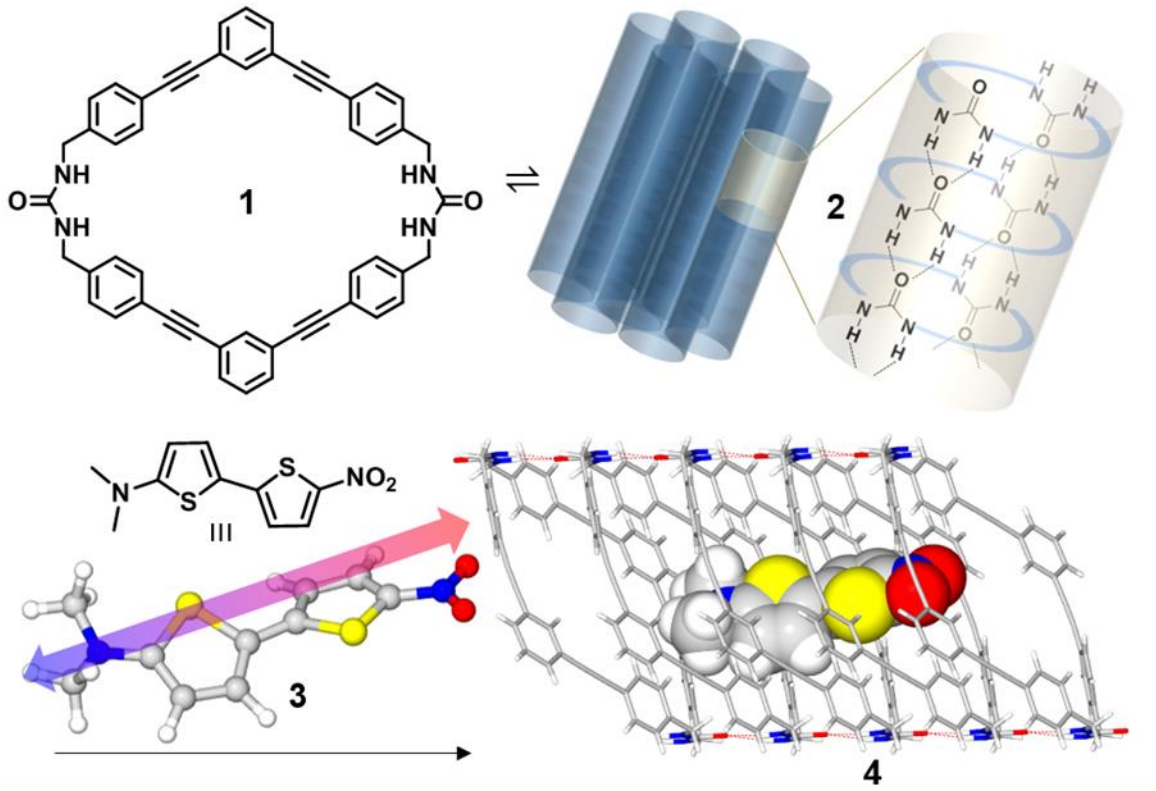

Figure 1.1 Dye uptake in one-dimensional macrocycle channels. Macrocycle **1**crystallizes into columnar fibers **2** from DMSO. After DMSO removal, equilibration with dye **3** affords the host–guest complex **4**. Arrow superimposed on **3** indicates electronic transition dipole moment (EDTM) orientation.

CHAPTER 2

EXPERIMENTAL METHODS[2]

2.1 Materials and Instrumentations

All chemicals were purchased from Aldrich or VWR and used as received. Phenylethynylene bis-urea macrocycle[1] and 5-(dimethylamino)-5′-nitro-2,2′-bithiophene dye[18] were synthesized according to previously described procedures. ^{1}H NMR and ^{13}C NMR spectra were recorded on Varian Mercury/VX 300 NMR. Thermogravimetric analysis (TGA) was carried out using a TA Instruments SDT-Q600 simultaneous DTA-TGA. Solid-state diffuse-reflectance spectra were recorded using a PerkinElmer Lambda 35 UV–visible scanning spectrophotometer equipped with an integrating sphere. Fluorescence spectroscopy was carried out on an Edinburgh FS5 instrument equipped with a 150 W continuous wave xenon lamp source for excitation. Fluorescence lifetimes were measured using a Mini-τ lifetime spectrometer from Edinburgh Instruments equipped with a 300.6 nm picosecond-pulsed-light-emitting diode (EPLED 300). Wide-angle X-ray scattering (WAXS) was carried out using a SAXSLab Ganesha instrument. A Xenocs GeniX 3D microfocus source was used with a Cu target to generate a monochromatic beam

[2] Kittikhunnatham, P.; Som, B.; Rassolov, V.; Stolte, M.; Würthner, F.; Shimizu, L. S.; Greytak A. B. Fluorescence polarization measurements to probe alignment of a bithiophene dye in one-dimensional channels of self-assembled phenylethynylene bis-urea macrocycle crystals. *J. Phys. Chem. C* **2017**, *121* (33), 18102–18109. Reprinted here with permission of publisher.

with a 0.154 nm wavelength. A 300 K Pilatus detector (Dectris) was used to collect the two-dimensional (2D) WAXS patterns.

2.2 Preparation of Phenylethynylene Bis-Urea Macrocycle Host Fibers

Phenylethynylene bis-urea macrocycle **1** was synthesized following a previously reported four-step procedure (Scheme 2.1; sample ^{1}H and ^{13}C NMR spectra are shown in Figures 2.1 and 2.2, respectively). The macrocycle (150 mg) was dissolved in DMSO (30 mL) at 120 °C, hot filtered, and cooled to room temperature at 1 °C/h to afford microcrystalline fibers **2** after 5 days, with typical diameters of 2–7 μm and lengths of 10–70 μm. The channels of **2** are not empty but are filled with DMSO solvent molecules in a 1:1 host:guest stoichiometry represented schematically in Figure 2.3. To permit the exchange of DMSO for other guests, **2** was activated by heating. The temperature of the unactivated host fibers was raised from 25 to 170 °C at a rate of 4 °C/min and held at 170 °C for 10 min, then the samples were slowly cooled to room temperature under He (g). This process was monitored using TGA, which shows a two-step desorption curve between 30 and 130 °C with a weight loss of 18.38% (Figure 2.3) corresponding to the removal of DMSO.

2.3 Preparation of Host–Guest Fibers

Host fibers **2** (3.8 mg, containing 5.24×10^{-6} mol **1**) were immersed overnight in a 0.94 mM solution of **3** (1.10×10^{-5} mol total) in degassed acetonitrile. The sample was then washed with cyclohexane on a suction filter and dried under vacuum to give the host–guest complex **4** as a purple solid.

2.4 Thermogravimetric analysis calculation

The ratio of macrocycle **1** to DMSO in host fibers prior to activation was calculated to be 1:2 using the formulas below:

$$\text{Moles of host} = \frac{\text{Final weight (g)}}{724.2845\ (\frac{\text{g}}{\text{mol}})}$$

$$\text{Moles of guest} = \frac{\text{Initial weight-Final weight (g)}}{\text{Guest molecular weight}\ (\frac{\text{g}}{\text{mol}})}$$

$$\text{Host : Guest} = \frac{\text{Moles of host}}{\text{Moles of guest}}$$

2.5 Fluorescence Polarization Measurements

An Olympus BX-51 epifluorescence microscope equipped with a 120 W metal halide excitation lamp was used for polarized fluorescence microscopy of single fibers. A UV excitation filter cube (Olympus U-MWU2), a green excitation filter cube (Olympus U-MNG2), a fixed excitation linear polarizer (Olympus U-PO3), and a rotatable linear analyzer (emission polarizer) were used with a 20× objective lens (0.45 NA). Images were collected with a color digital CMOS camera (Canon EOS REBEL T3/1100D) operated in a linear response mode. Samples of macrocycle fiber crystals were mechanically transferred to a microscope slide using a needle tip, and the slide was then placed on a rotatable stage. Typically, several nonoverlapping fibers with easily identifiable orientations could be found within the field of view. The fluorescence intensity above background of the host and host–guest complex fibers and the orientation of the fiber axis relative to the polarizers were measured from RGB color micrographs using a profile analysis method described previously.[37] In particular, for each fiber studied, a profile line was drawn orthogonal to the fiber axis, including a portion of the background on either

side. The profile was expanded along the fiber axis into a rectangular region of interest. Pixel intensity values sampled within this region of interest were averaged along dimensions parallel to the fiber axis and then plotted as a function of position along the orthogonal dimension. The integrated peak area above the baseline set by the background regions at each end of the plot was used to define the intensity. We used a similar approach to study inorganic nanowires.[37] Details of the microscope configuration are shown in Figure 2.4.

Fluorescence lifetime calculations

Fluorescence decay lifetimes of host **2** and host-guest complex **4** were measured using a Mini-τ lifetime spectrometer from Edinburgh Instruments equipped with a 300.6 nm picosecond-pulsed-light-emitting diode (EPLED 300). The lifetimes and decay profiles are shown in Table 3.1 and Figure S6. The amplitude-weighted average lifetime τ_{av} is the appropriate measure by which to describe fluorescence resonant energy transfer.[43] Accordingly, the decays were fit with a triexponential function (n = 3), where τ_i and B_i are respective lifetimes and amplitudes of each component, and these fit parameters were used to calculate τ_{av}:

$$\text{Fit: } A+B_1\cdot e^{(-t/\tau_1)}+B_2\cdot e^{(-t/\tau_2)}+B_3\cdot e^{(-t/\tau_3)}$$

$$\tau_{av}=\frac{B_1\tau_1+B_2\tau_2+B_3\tau_3}{B_1+B_2+B_3}$$

The energy transfer efficiency, Φ_{ET} was calculated using the following equation:

$$\Phi_{ET}\ [\%]=\frac{k_{et}}{k_r+k_{nr}+k_{et}}=\frac{k_{et}}{k_o+k_{et}}$$

The k_o and k_{et} values are obtained from the decay lifetimes for donor molecule (τ_D) and donor molecule in the presence of acceptor ($\tau_{D\text{-}A}$), which are $\tau_D = 1/k_o$ and $\tau_{D\text{-}A} = 1/(k_o + k_{et})$, respectively. The calculated Φ_{ET} was 14.8%.

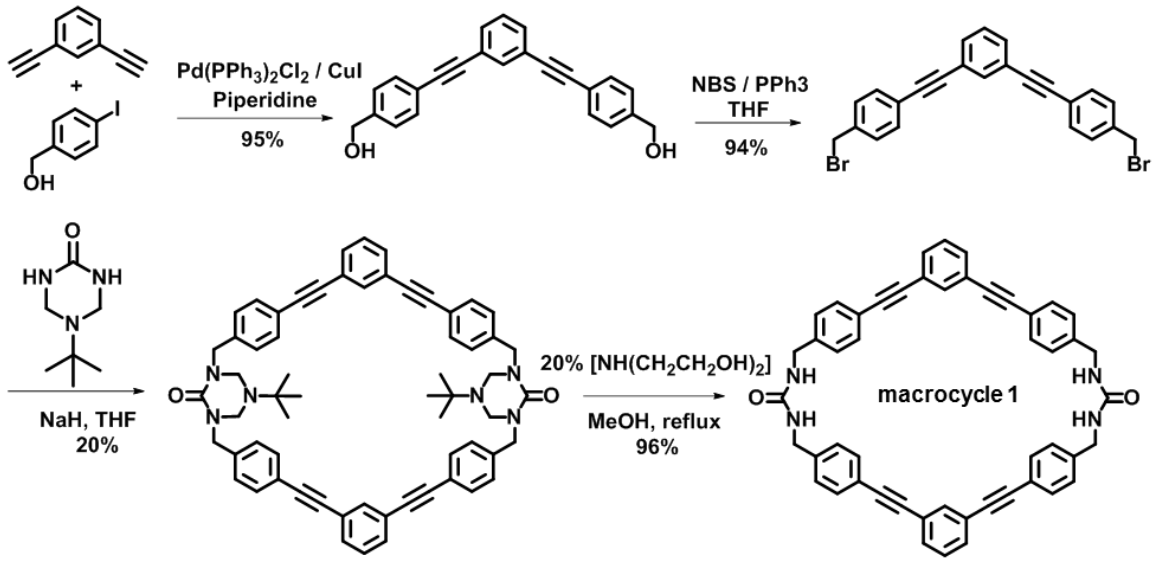

Scheme 1 An overview of phenylethynylene *bis*-urea macrocycle synthesis.[1]

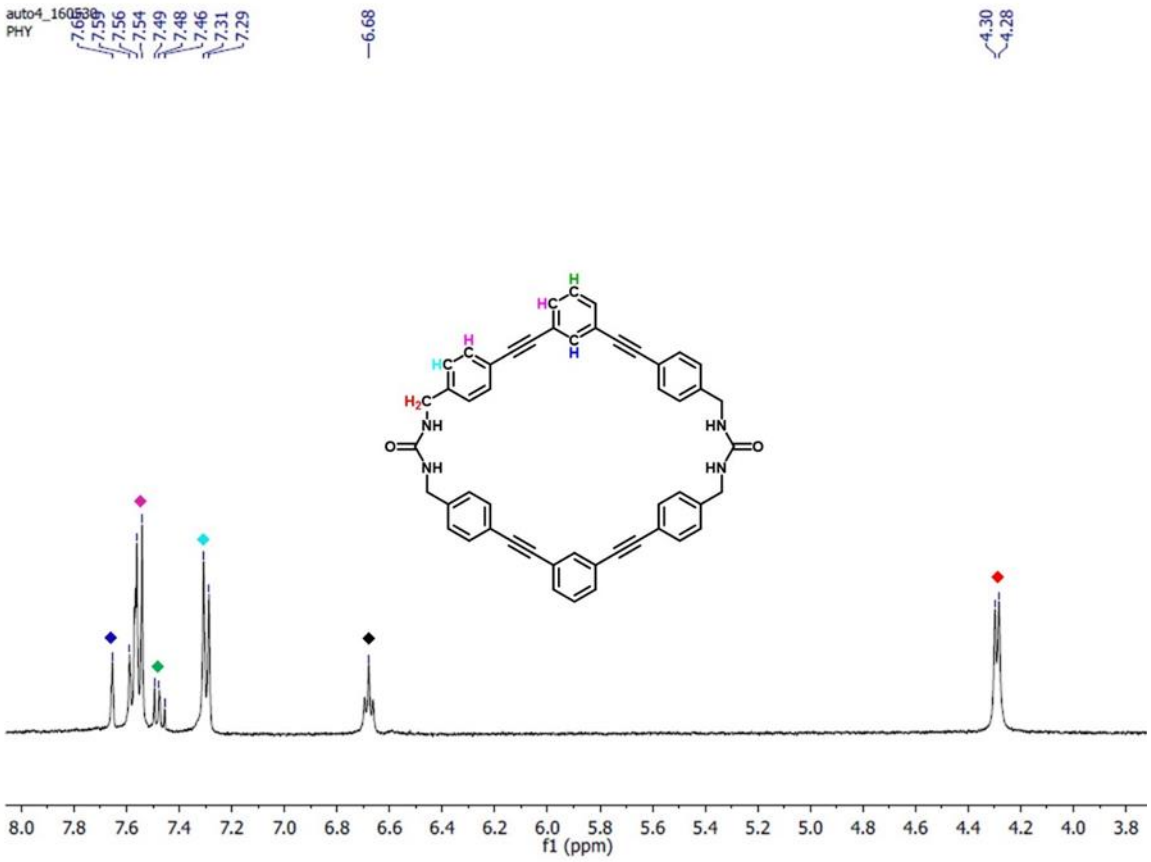

Figure 2.1 ^{1}H NMR spectrum of host **2** dissolved in DMSO-d_6 (400 MHz): 7.64 (s, 2H, Ar-H), 7.55 (m, J=20.0 Hz, 12H, Ar-H), 7.47 (t, J=16.0 Hz, 2H, Ar-H), 7.28 (d, J=8.0 Hz, 8H, Ar-H), 6.69 (t, J=12.0 Hz, 4H, -NH), 4.28 (d, J=8.0 Hz, 8H, -CH2).

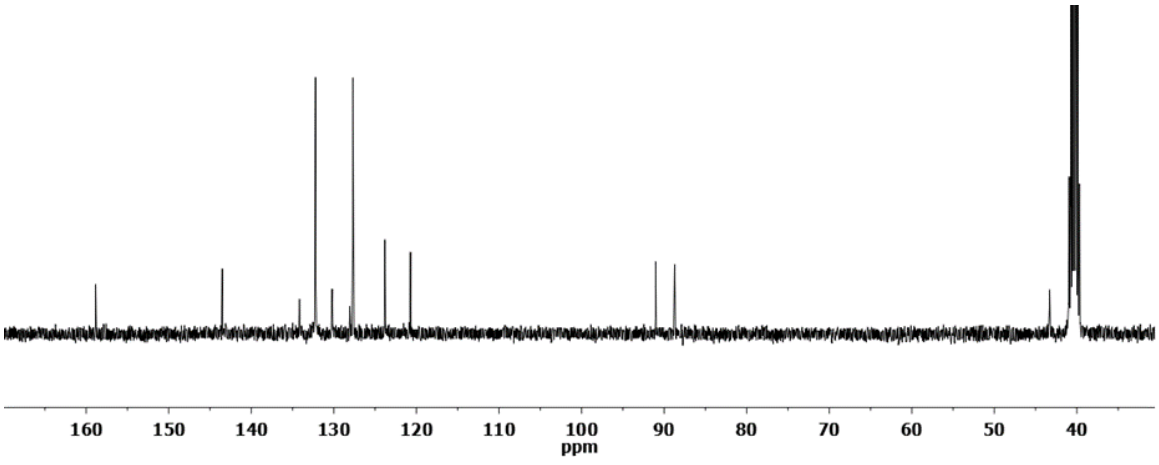

Figure 2.2 ^{13}C NMR spectrum of host **2** dissolved in DMSO-d_6 (100 MHz): 158.9, 134.5, 134.2, 132.3, 130.2, 128.1, 127.7, 123.8, 120.7, 91.0, 88.7, and 43.3.

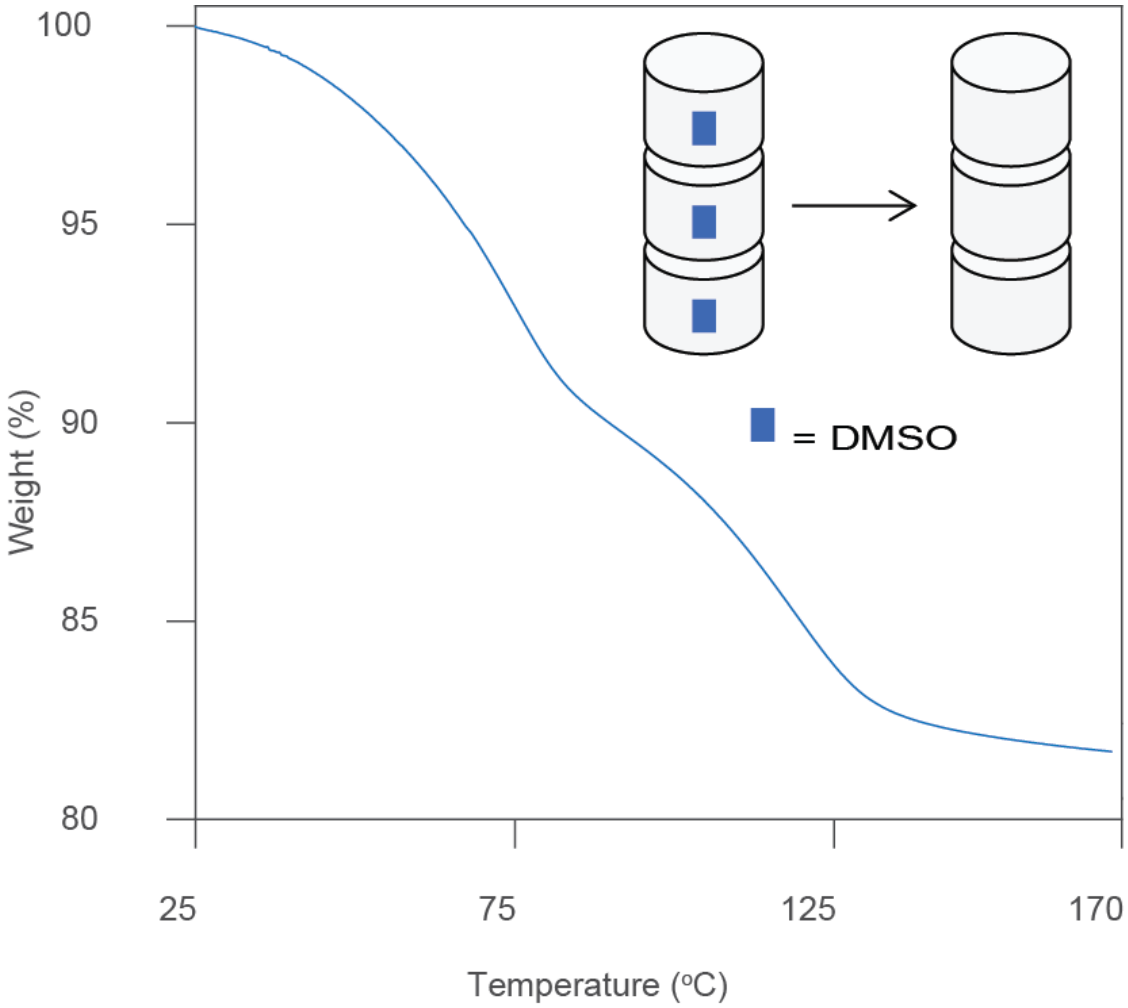

Figure 2.3 Activation of host **2** by TGA shows a two-step desorption curve corresponding to the removal of DMSO guest.

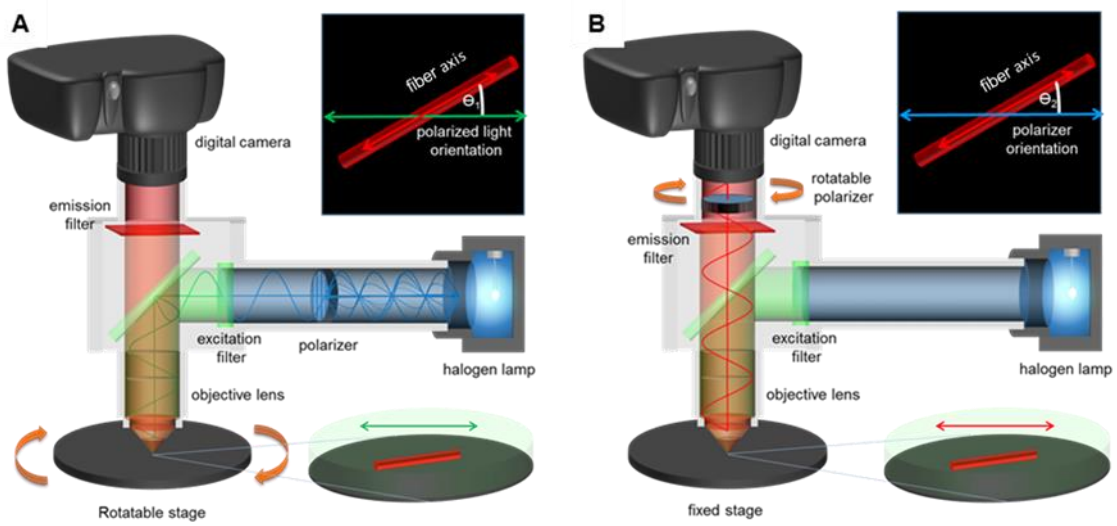

Figure 2.4 Experimental setups for fluorescence polarization microscopy measurements. In the excitation polarization measurement (A), no emission polarizer is used. Then, the sample was illuminated with linearly polarized excitation at 530-550 nm (green excitation filter cube), or at 330-385 nm (uv excitation filter cube) through the objective lens. In this measurement, the orientation of the polarized excitation was fixed and the sample was rotated to collect a series of fluorescence micrographs of the sample showing the fibers with varying angles between fiber axes and polarized excitation light direction (θ_1). A matching image with unpolarized excitation was used for signal correction at each sample position. In the emission polarization measurement (B), unpolarized excitation is used, and the emission polarizer (analyzer) is rotated through a series of angles while the sample remains fixed. Matching unpolarized images, taken with the analyzer withdrawn, were used for signal correction. This gives a series of measurements with varying angles between the fiber axes and the emission polarizer axis (θ_2).

CHAPTER 3

RESULTS AND DISCUSSION[3]

Treatment of activated host crystals **2** with solutions of **3** in acetonitrile led to uptake of the dye. A color change from white to purple was visible to the naked eye and in transmission micrographs of individual crystals as illustrated in Figure 3.1. Figure 3.1 compares the crystals before and after dye exposure. To control for the possibility of surface adsorption, the unactivated fibers **2**·DMSO were similarly immersed in dye solution but displayed no coloration, suggesting that the majority of the dye molecules in complex **4** are incorporated in the channels and are not on the surface. Dye **3** was also not absorbed by samples in which the host channels were occupied by the previously characterized chromone guest.

To quantify the loading of the dye, complex **4** was disassembled by dissolution in DMSO-d_6 to afford the free macrocycle **1** and the dye and analyzed by ^{1}H NMR (Figure 3.2). Comparison of the integration of the methylene CH_2 from **1** and the CH_3 from the dye **3** gave a ratio of 11.0:1. The average host:guest ratio for 3 loading experiments was 10.8:1. The loading for **3** was lower than that for previously reported polar guest 3-cyano

[3] Kittikhunnatham, P.; Som, B.; Rassolov, V.; Stolte, M.; Würthner, F.; Shimizu, L. S.; Greytak A. B. Fluorescence polarization measurements to probe alignment of a bithiophene dye in one-dimensional channels of self-assembled phenylethynylene bis-urea macrocycle crystals. *J. Phys. Chem. C* **2017**, *121* (33), 18102–18109.
Reprinted here with permission of publisher.

chromone (2:1 host:guest).[2] Dye **3** is significantly larger than the chromone (281.1 vs 197.5 Å^3) and, based on the structural model, the loading ratio appears to represent about 50% of the available space.

Previously, the crystallinity of **2** and host–guest derivatives were probed by X-ray techniques, including powder X-ray diffraction (PXRD).[1] Given the small sample size,WAXS was used to probe the structure of host–guest complex **4**. In Figure 3.host **2** shows a sharp WAXS pattern between 2θ = 2–25°, similar to PXRD patterns previously reported for this homogeneous crystalline material. Comparison of the WAXS pattern of activated **2**, dye **3**, and complex **4** suggests that the complex is not a simple mixture of the two components (Figure 3.4). Upon dye complexation, **4** maintains many of the key sharp peaks in **2**, including the low angle peaks at 2θ = 5.94, 9.64, and 15.01°, while slight shifting was observed in several peaks between **2** (7.05 and 11.21°) and complex **4** (6.77 and 11.30°), suggesting that high crystallinity is maintained upon uptake of the dye into the 1D pores while accommodating some changes in the overall structure.

In comparison to guests previously loaded into host **2**, the bithiophene dye **3** is more polar (7.95 D) and shows a marked solvotochromism. The peak energy has previously been shown[18, 19] to vary linearly with Kamlet and Taft's polarity parameter π*.[38, 39] For example, in Figure 3.5 we compare the absorption spectra of **3** in four solvents of different polarities. The peak shifts to longer wavelengths as the solvent π* increases, from λ_{max} = 467 nm in hexanes (π* = −0.08) to λ_{max} = 498 nm in diethyl ether (Et_2O, π* = 0.27) to λ_{max} = 533 nm in acetonitrile (CH_3CN, π* = 0.75) to λ_{max} = 562 nm in dimethyl sulfoxide (DMSO, π* = 1.00), similar to previous measurements.[18] This sensitivity to solvent

polarity should provide a measure of the interior environment of the channels. Fluorescence spectra of **3** in the four solvents show a similar shift (Figure 3.6); the emission peak of the dye **3** shifts from 521 nm in hexanes to 693 nm in DMSO ($\lambda_{exc} \sim 530–550$ nm). However, in highly polar solvents (e.g., CH_3CN and DMSO), the photoluminescence intensity of the dye **3** is significantly quenched; no photoluminescence peak of the dye **3** was detected in CH_3CN under 530 nm excitation.

Figure 3.7 compares the diffuse reflectance and fluorescence spectra of **2** and host–guest complex **4**. Host **2** exhibits a broad absorption band with $\lambda_{max} = 322$ nm. In comparison, the host–guest complex displays two absorption bands. The band attributed to the host at $\lambda_{max} = 327$ nm is slightly red-shifted from that of the free host. A second, more intense band is observed at 552 nm, which is attributed to dye **3**. Comparison of these results to reported UV–vis absorption maxima suggests that the interior environment of the channel exhibits $\pi^* \approx 0.90$, comparable to dimethylformamide, based on the polarity scale established previously for this probe.[18]

Figure 3.7 also shows emission spectra of **2** and host–guest complex **4** obtained by exciting the samples at 280 nm. This excitation wavelength was selected to preferentially excite the host, as it is well below the absorption maximum of the dye in representative organic solvents. Host **2** has an emission maximum at 404 nm, while the host–guest **4** emission maxima are at 400 and 649 nm. The peak at 649 nm is attributed to the guest and lies within the range found for **3** in polar solvents. Unactivated fibers did not display this fluorescence peak after exposure to a solution of **3** (Figure 3.8). Guest emission can arise both from direct excitation and by energy transfer (ET) from the host. In the case of efficient nonradiative energy transfer from the host to the guest, a reduction in the

average decay lifetime of the host is expected. While **2** and **4** both showed multiexponential decays, the amplitude average lifetime decreased from 1.27 to 1.08 ns, indicating energy transfer efficiency up to ~15% (Figure 3.9 and Table 3.1).

Because the length of guest **3** exceeds the diameter of the 1D channels in the host, we expect that a limited range of orientations is accessible to the guest, within which rotational diffusion may occur. The distribution of molecular orientations that is accessible to the guest can be probed experimentally via fluorescence polarization measurements. In a simplistic model, molecular orientations in a cylindrical channel can be thought of as having a cone-like distribution in which excursions beyond a characteristic tilt angle α are inaccessible. In the case of host **2**, the available crystal structure allows us to make some general arguments about the symmetry of the distribution about the axis and to investigate the influence of specific interactions between the host and guest through density functional theory calculations.

The unit cell of the host crystal actually encompasses two unique, parallel 1D channels that are rotated by 180° from each other about the channel axis. Additionally, within each channel, the macrocycles are stacked such that the urea carbonyls point in opposite directions on opposite sides of the channel. As a result, as shown in Figure 3.10, any particular guest site within a channel is representative of four symmetrically equivalent sites in the crystal structure. Guests occupying equivalent sites in neighboring channels have equal and opposite tilt angles with respect to the channel axis. As a result, the observed polarization axis in fluorescence measurements is expected to coincide with the channel axis; however, the magnitude of the polarization will depend on the distribution of tilt angles that are thermally accessible.

DFT calculations with ADF2014[40] were used to investigate the feasibility of loading dye **3** into the channels and to evaluate the geometry of the encapsulated guest. The host model was generated by importing the atomic coordinates from the single crystal X-ray structure of the host, omitting the coordinates of the solvent guests and truncating the structure to five macrocycles of a single column. The long axis of the guest molecule **3** is larger than the host channel inner diameter (11 vs 9 Å internuclear distance), suggesting a lengthwise orientation. From an initial starting position, the geometry of the guest molecule was optimized at the PBEsol-D3/DZP level, keeping the host geometry frozen. Figure 3.11 depicts the optimized geometry of the host–guest complex **4** and indicates that the long axis of the guest molecule **3** aligns approximately parallel to the host channel axis and that a minimum of four macrocycles are needed to fully encapsulate the dye (optimized coordinates are provided in Table A1). In the optimized structure, the molecule is slightly off center due to favorable interactions with the host sidewall. We next carried out a TDDFT calculation at the B3LYP/TZ2P level to confirm the orientation of the lowest-energy electronic transition dipole moment (ETDM) in the guest.

The orientation of the calculated ETDM of the guest in the optimized structure is nearly parallel to the plane defined by the urea oxygen atoms of the host and is canted by and angle $\alpha = 9.5°$ from the channel axis, as represented by the arrow in Figure 3.11. While this represents the optimized guest geometry, thermal population of higher energy geometries may occur at room temperature. To evaluate this possibility, we performed a geometry optimization calculation with the molecule constrained to interact with the two opposing sides of the host channel. This calculation yielded a guest structure in which the calculated EDTM is tilted at an angle $\alpha = 30°$ from the channel axis and with the ground

state energy only 175 K, or 0.35 kcal/mol, above the optimized minimum. It is likely that there are many similar states within the thermally accessible energy from the minimum, leading to a broad distribution of ETDM orientations with $\alpha \leq 30°$ at room temperature.

On the basis of the diffuse reflectance and fluorescence data, appropriate excitation and emission channels were selected for polarimetric fluorescence microscopy of individual macrocycle fibers cast on glass substrates. A green excitation filter cube (530–550 nm excitation band-pass; 570 nm dichroic mirror, 590 nm emission long-pass filter) was use to selectively excite the guest. For comparison, a UV excitation filter cube (330–385 nm excitation band-pass; 400 nm dichroic, 420 nm emission long-pass) is used to excite the host and guest together with separation of host and guest emission signals possible through the use of a color camera. These excitation and emission conditions were combined with linear polarizers to perform fluorescence excitation and emission polarization measurements to assess the orientation of the dye within the 1D channels. Details of the experimental setup are shown in Figure 2.4.

In the excitation polarization measurement, linearly polarized light is used to excite the sample. The fiber axis is rotated with respect to the polarization vector of the incident light. No polarizer is applied to the emission such that all light emitted toward the objective lens is collected. Excitation polarization is sensitive to the anisotropy of the transition dipole alignment in the absorbing state: the excitation rate is greatest if the polarizer is parallel to the excitation dipole and reaches a minimum if they are perpendicular. If this is the same state from which light is emitted, the information is the same as for emission anisotropy, but in the case of significant relaxation or energy transfer between the absorbing and emitting states, the excitation anisotropy may be diminished. Measurements

were performed simultaneously on multiple fiber-like crystals within the field of view of the microscope by recording a series of images at different angles and then determining the crystal orientation and fluorescence intensity above background. Figure 3.12A–D are fluorescence micrographs illustrating excitation polarization in a representative host–guest complex fiber **4** (profile 1 in Figure 3.14) with the green excitation filter cube. To correct for any effects of photobleaching, uneven detector response, or instability of the light source throughout the experiment, the fluorescence intensities were normalized by comparison to matching images recorded with both polarizers removed (Figure 3.12A and C). The arrows show the orientation of the polarized excitation. From the micrographs, the brightness of the host–guest complex fiber when the excitation light is polarized parallel to the fiber axis is greater than when the excitation light is polarized perpendicular to the fiber axis. To analyze the excitation polarization anisotropy in greater detail, I_θ/I_{max} was plotted as a function of the angle θ_1 between the direction of the polarized excitation and the direction of the fiber axis (Figure 3.12E), where I_θ is the ratio of fluorescence intensity of the fiber when excited by linearly polarized light to fluorescence intensity of the fiber excited by unpolarized light and I_{max} is the maximum value of I_θ. From the plot, a large oscillation is evident. I_θ/I_{max} is highest when the direction of the polarized excitation is parallel to the fiber axis ($\theta_1 \approx 0°$), whereas I_θ/I_{max} is minimized when the direction of the polarized excitation is perpendicular to the fiber axis ($\theta_1 \approx 90°$).

A similar response is observed for emission polarization in the host–guest sample using the green (guest-selective) excitation channel (Figure 3.13). A series of fluorescence micrographs of the host–guest complex fibers was recorded with unpolarized excitation and observation through a linearly polarizing filter. As above, matching images with the

emission polarizer removed were used to normalize the intensity signals. Figures 3.13A–D are fluorescence micrographs of a representative host–guest complex fiber **4** (profile 8 in Figure 3.16) with unpolarized excitation and different emission polarizer conditions. Plotting I_θ/I_{max} as a function of emission polarizer angles θ_2 relative to the fiber axis (Figure 3.13E) indicates strongly polarized light emitted from the host–guest complex fiber **4**.

In analyzing fluorescence polarization data, we aim to determine if a preferential (i.e., nonrandom) distribution of molecular orientations exists and, if so, the relationship between that distribution and the crystal axis. The polarization *P* of a fluorescent emitter is classically defined[41] based on the intensities of components with electric field parallel or perpendicular to an axis of reference, here the observed long axis of the crystal:

$$P = \frac{I_{\parallel} - I_{\perp}}{I_{\parallel} + I_{\perp}} \tag{3.1}$$

If all dipoles are aligned with the crystal axis, *P* will approach 1, but disorder among dipole orientations and unpolarized background contributions will lead to diminished values of *P*.

The measured intensity is expected to vary sinusoidally as θ_1 or θ_2 is changed, with a period of 180°. Symmetry arguments based on the crystal structure, as outlined above, indicate that any net polarization due to alignment of guests must lie parallel to, or perpendicular to, the crystal axis. However, our data analysis considers the possibility that the angle of maximum intensity is offset from the crystal axis by an angle ϕ, such that the relative intensity I_θ/I_{max} is described by

$$\frac{I(\theta)}{I_{max}} = I_n + I_p \cos^2(\theta + \phi) \tag{3.2}$$

where I_n and I_p represent the relative intensities of a "normal" (unpolarized) component of the signal and of a component that is linearly polarized with a maximum at $\theta = \phi$, respectively. These can be combined to give a single value $P_{max} = I_p/(I_p + 2I_n)$ that represents the maximum polarization that would be observed using polarizers aligned with the transition dipole projection. A least-squares fit of the experimental data to eq 3.2 provides values of P_{max} and ϕ for each macrocycle crystal. It is also possible to obtain, from the fit, values of $I_{\parallel}$ and $I_{\perp}$ that may be substituted into eq 3.1 to give:

$$P = P_{max} \cos 2\phi \tag{3.3}$$

This is valuable because, while P_{max} is always positive, measurements of P are expected to be zero-centered in the absence of significant anisotropy, and as such the distribution of P values measured for multiple individual crystals in the sample can be used to detect statistically significant excitation or emission polarization in the case of weak modulation or noisy signals. In the case that significant polarization is found, as is the case for the examples in Figures 3.12 and 3.13, the value of P_{max} can be used to characterize the amount of disorder that could be present in ETDM orientations in the absence of rotational diffusion. Including the parameter ϕ also allows P_{max} to be measured accurately in the event of small errors in assignment of the fiber orientation with respect to the polarizers.

Excitation polarization in the guest-selective (green) channel (Figure 3.12) was measured for seven single host–guest fibers (see Figure 3.14). Plots of I_θ/I_{max} versus θ_1 obtained from each fiber are well-fit by eq 3.2 (Figure 3.15). Among the crystals analyzed, $P_{max} = 0.65 \pm 0.05$, rising to a maximum of 0.715 and $\phi = 0.1 \pm 1.4°$, where uncertainties represent sample standard deviations. For emission polarization under guest-selective excitation (Figure 3.13), a total of nine host–guest complex fibers (Figures 3.16

and 3.17) were investigated using the same method. Plots of I_θ/I_{max} versus θ_2 reveal P_{max} = 0.56 ± 0.14 (max 0.729) and ϕ = 7.4 ± 11.6°. The consistent observation of significant fluorescence polarization of the dye in **4** helps to confirm that the guest occupies the 1D channels in the host. In analyzing the magnitude of the polarization as a probe of guest orientation, it is important to consider trivial causes of depolarization, which include common mode background contributions and scattering or attenuation of excitation or fluorescence light. The profile analysis method eliminates background that is not uniquely associated with the fiber. However, a nonzero host fluorescence signal (analyzed below) exists in addition to probe fluorescence. As can be seen in Figure 3.1, some attenuation of visible light is noticeable in the dye-loaded fibers; based on the observed excitation polarization, such absorption will tend to selectively attenuate excitation light with polarization parallel to the fiber axis. Because of these factors, we considered the maximum observed P_{max} as a point of comparison with calculated results. In a cone model (see Appendix A), P_{max} = 0.729 requires $\alpha < 29°$ for dipoles at a fixed angle α, or $\alpha_{max} < 42°$ for a static square well (the addition of diffusion, i.e. a "wobbling cone", had little effect: $\alpha_{max} < 43°$). We note that a fixed angle of 9.5°, as found in the minimized structure, gives P_{max} = 0.97. The diminished experimental result for P_{max} could indicate that the larger accessible angle, in which the guest spans the channel to interact with both sides, is predominant at room temperature.

We additionally examined fluorescence anisotropy in dye-free crystals of the host **2**. Excitation using the green filter cube (Figures 3.18 and 3.19), which has minimal overlap with the host absorption spectrum, produced weak fluorescence with no significant emission polarization: P = 0.08 ± 0.13, where the uncertainty represents a 95% confidence

interval for the average value (Figure 3.13). Excitation of **2** with the UV filter cube (Figures 3.20 and 3.21) produced stronger fluorescence centered in the blue channel as expected from the ensemble fluorescence spectrum. A small but significant emission polarization was detected in this case with the maximum polarization axis ϕ again close to zero.

With the behavior of the dye-free host **2** established, we revisit the case of the host–guest crystals **4** under UV excitation. In this mode, a majority of the total light emitted comes from the host; however, the guest contributes as well due to direct excitation and energy transfer as discussed above. We observed a small but significant emission polarization when the total visible light fluorescence channel is considered (Figures 3.22 and 3.23), as shown in Figure 3.28. Considering the red and blue channels of the color micrographs separately (Figures 3.24 and 3.25), a larger polarization was seen in the red channel where guest emission contributes most strongly. On the other hand, excitation polarization in **2** was weak and could not be statistically distinguished from zero (Figures 3.26 and 3.27). These two results suggest a picture in which degenerate or overlapping ETDMs in the host in the UV region lead to scrambling of the incident excitation polarization prior to energy transfer to the guest. However, emission ultimately emerging from the guest remains polarized along the crystal axis, contributing to the significant emission polarization observed in the red channel upon UV excitation. We note that the large difference in the extent of fluorescence anisotropy between the visible and UV channels suggests that dielectric contrast, seen previously in polarization measurements on inorganic semiconductor nanowires,[36] is not a major contribution in the present case.

Table 3.1 Life times of host **2** and host-guest complex **4**.

	Host 2	Host-guest complex 4
$B_1(X\ 10^{-2})$	8.16	9.29
$B_2(X\ 10^{-2})$	2.37	1.94
$B_3(X\ 10^{-2})$	0.23	0.17
τ_1 (ns)	0.68	0.63
τ_2 (ns)	2.56	2.36
τ_3 (ns)	8.86	11.12
τ_{av} (ns)	1.27	1.08
χ^2	1.19	1.27

Table 3.2 Summary of data from polarization measurements.

Measurement	Sample	Excitation Channel	Emission Channel	P_{avg} [a]	$P_{max,avg}$	Φ (degrees)	
						avg	std dev
Emission polarization	host-guest	green filter cube[b]	rgb	0.531 ± 0.143	0.562	7.4	±11.6
		uv filter cube	rgb	0.065 ± 0.026	0.069	3.9	±10.3
			red	0.127 ± 0.044	0.130	-1.4	±7.5
			blue	0.058 ± 0.027	0.066	7.7	±16.8
	host (apo)	green filter cube	rgb	0.077 ± 0.126	0.087		
		uv filter cube	rgb	0.069 ± 0.044	0.077	0.5	±13.1
Excitation polarization	host-guest	green filter cube	rgb	0.645 ± 0.046	0.646	0.1	±1.4
		uv filter cube	rgb	0.040 ± 0.042	0.039		

[a] Uncertainties represent confidence intervals.
[b] Statistical results exclude profiles 3 and 4 in Figure 3.16 and 3.17

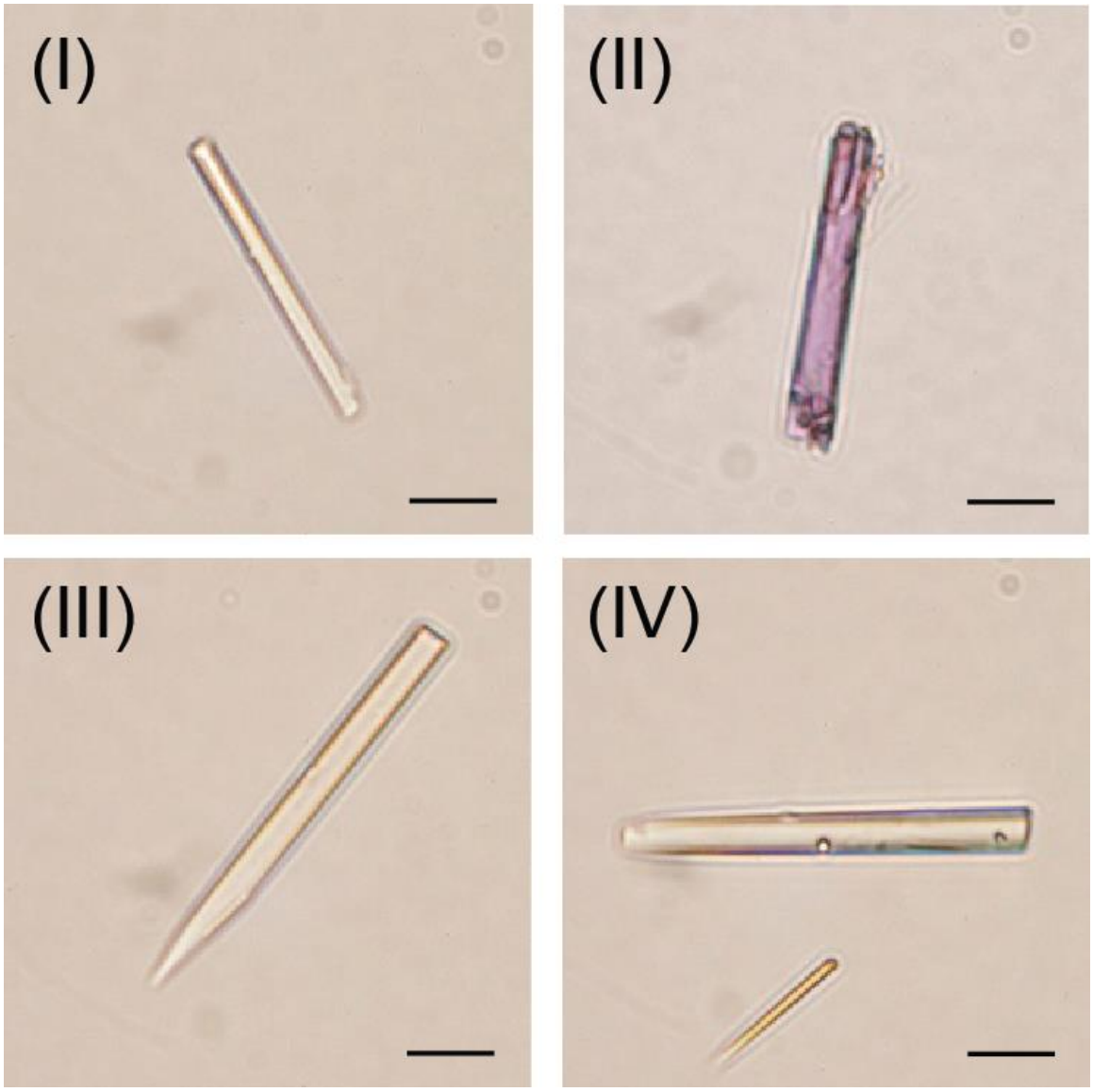

Figure 3.1 (I, II) Activated crystals before and after exposure to **3**. (III, IV) Unactivated crystals before and after exposure to **3**. Scale bars are 10 μm.

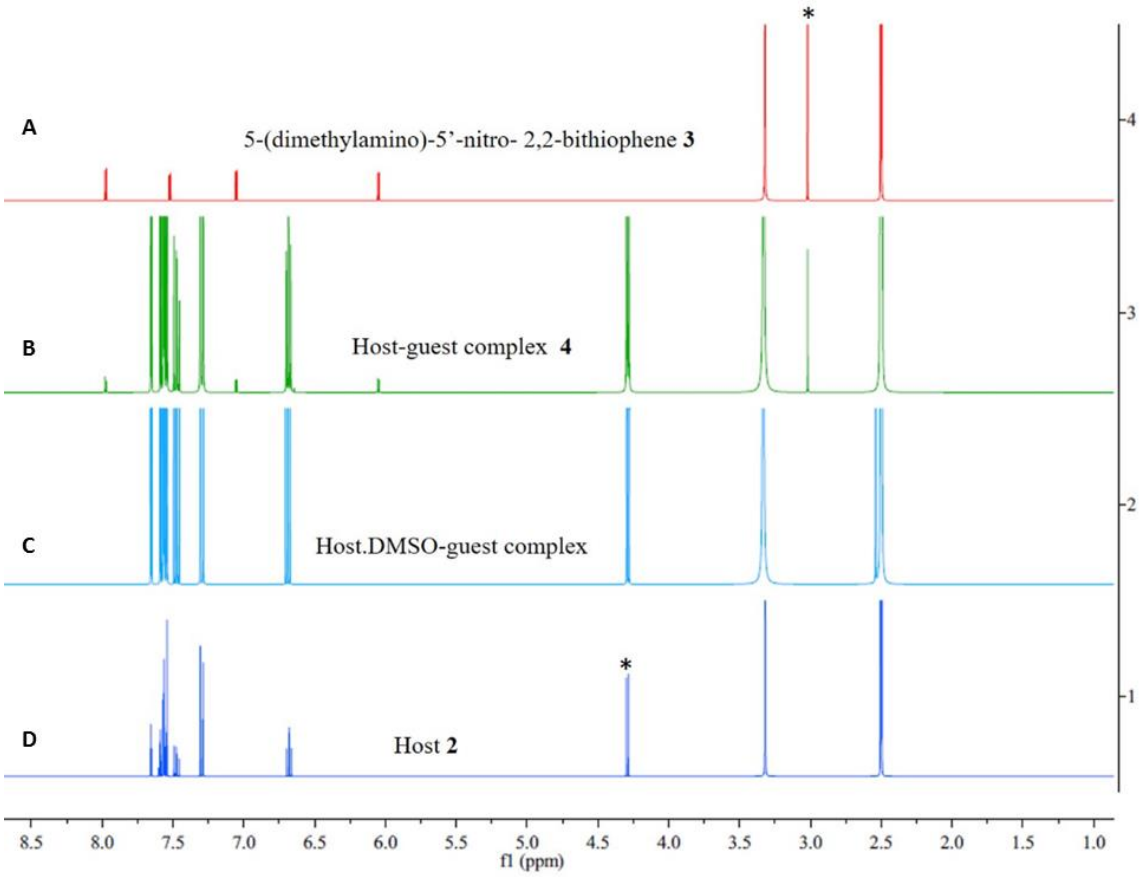

Figure 3.2 ^{1}H NMR spectra indicating the inclusion of dye **3** to host fibers **2.** ^{1}H NMR spectra of (A) dye **3** in DMSO-d_6, (B) host-guest complex **4** dissolved in DMSO-d_6, (C) unactivated host treated with dye **3** solution dissolved in DMSO-d_6, and (D) host fibers **2** dissolved in DMSO-d_6**.** The peaks corresponding to the dye appear in the ^{1}H NMR spectrum of host-guest complex **4** dissolved in DMSO-d_6 but do not appear in ^{1}H NMR spectrum of unactivated host treated with a solution of the dye dissolved in DMSO-d_6. These suggest that the dye molecule can diffuse into the empty host channel, but cannot diffuse into the host channel filled with DMSO molecule.

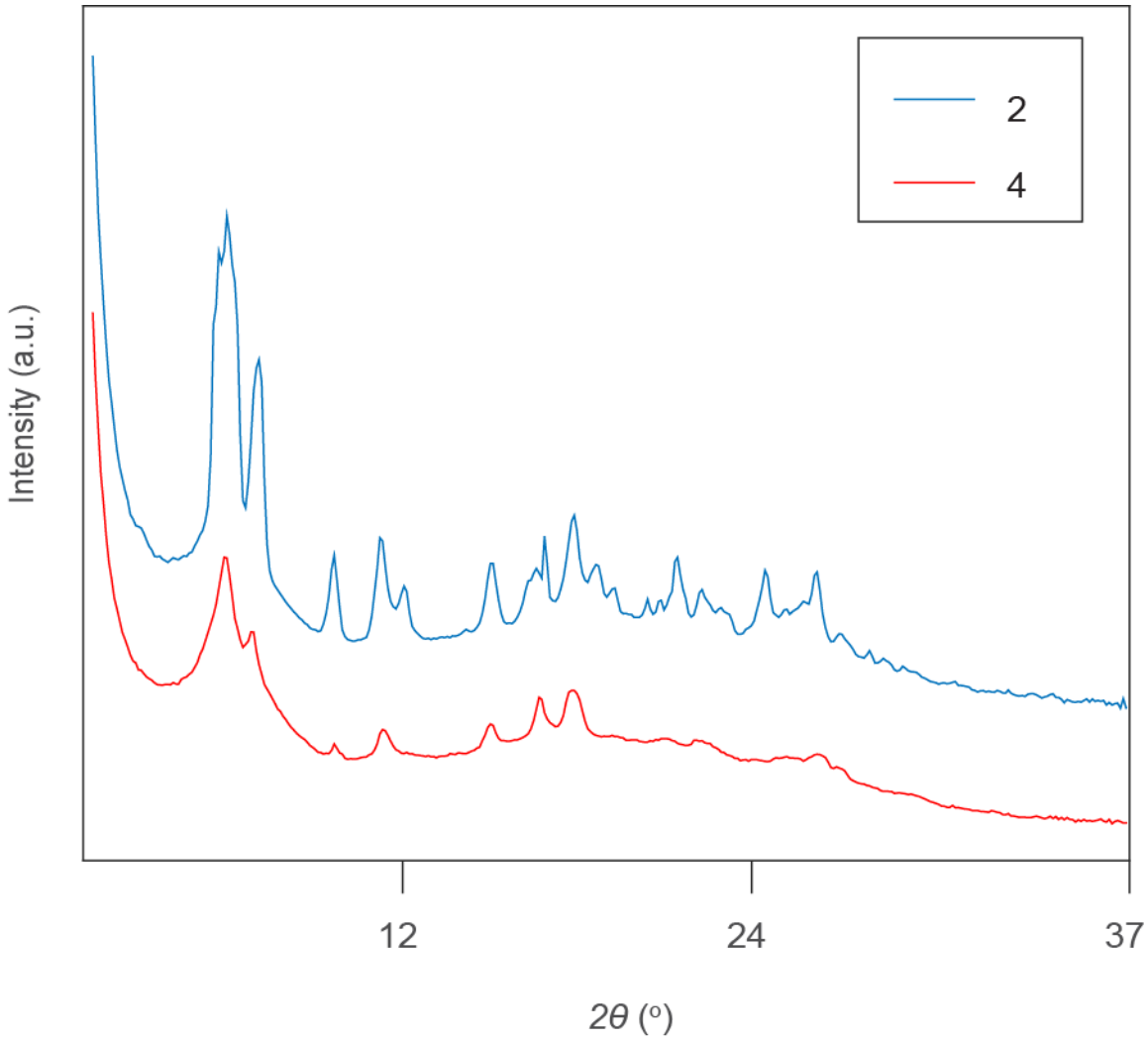

Figure 3.3 Normal-transmission WAXS patterns of **2** and **4**.

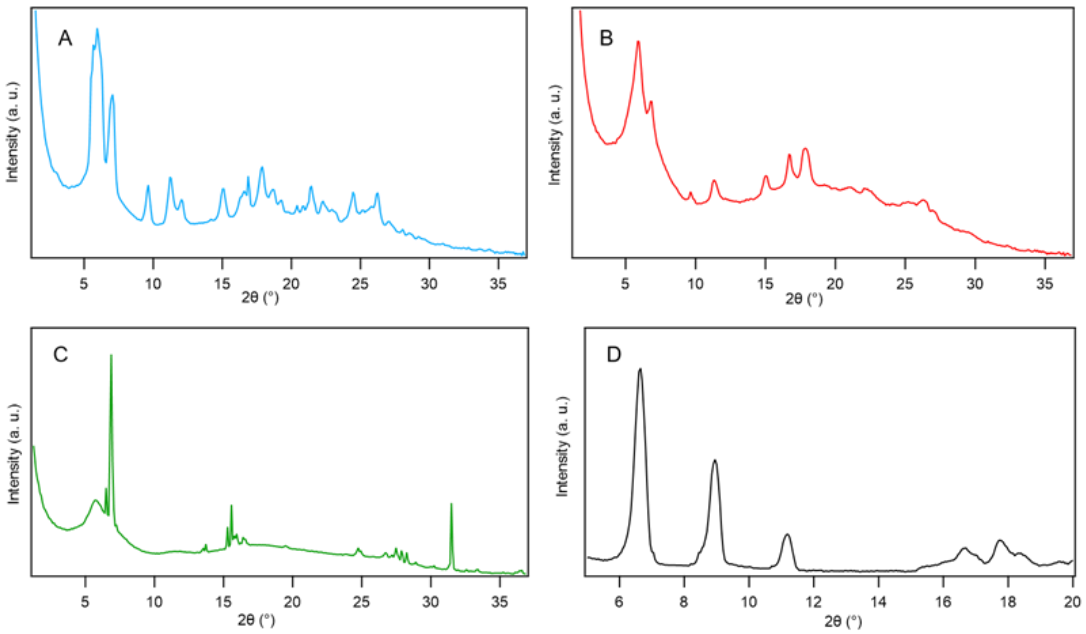

Figure 3.4 WAXS diffractograms of host fibers **2** (A), host-guest complex fibers **4** (B), 5-(dimethylamino)-5'-nitro- 2,2-bithiophene **3** (C), and PXRD pattern of host fibers **2** (D)[1] demonstrating morphological integrety of the host fiber. 2θ positions (°) of major peaks; (A): 5.94, 7.05, 9.64, 11.21, 15.01, 16.87, 17.90, 21.45, 24.46, 26.25, (B): 5.94, 6.77, 9.64, 11.30, 15.01, 16.69, 17.80, 21.08, 22.11, 26.25, (C): 5.76, 6.87, 15.57, 31.48, and (D): 6.65, 8.95, 11.20, 16.65, 17.7.

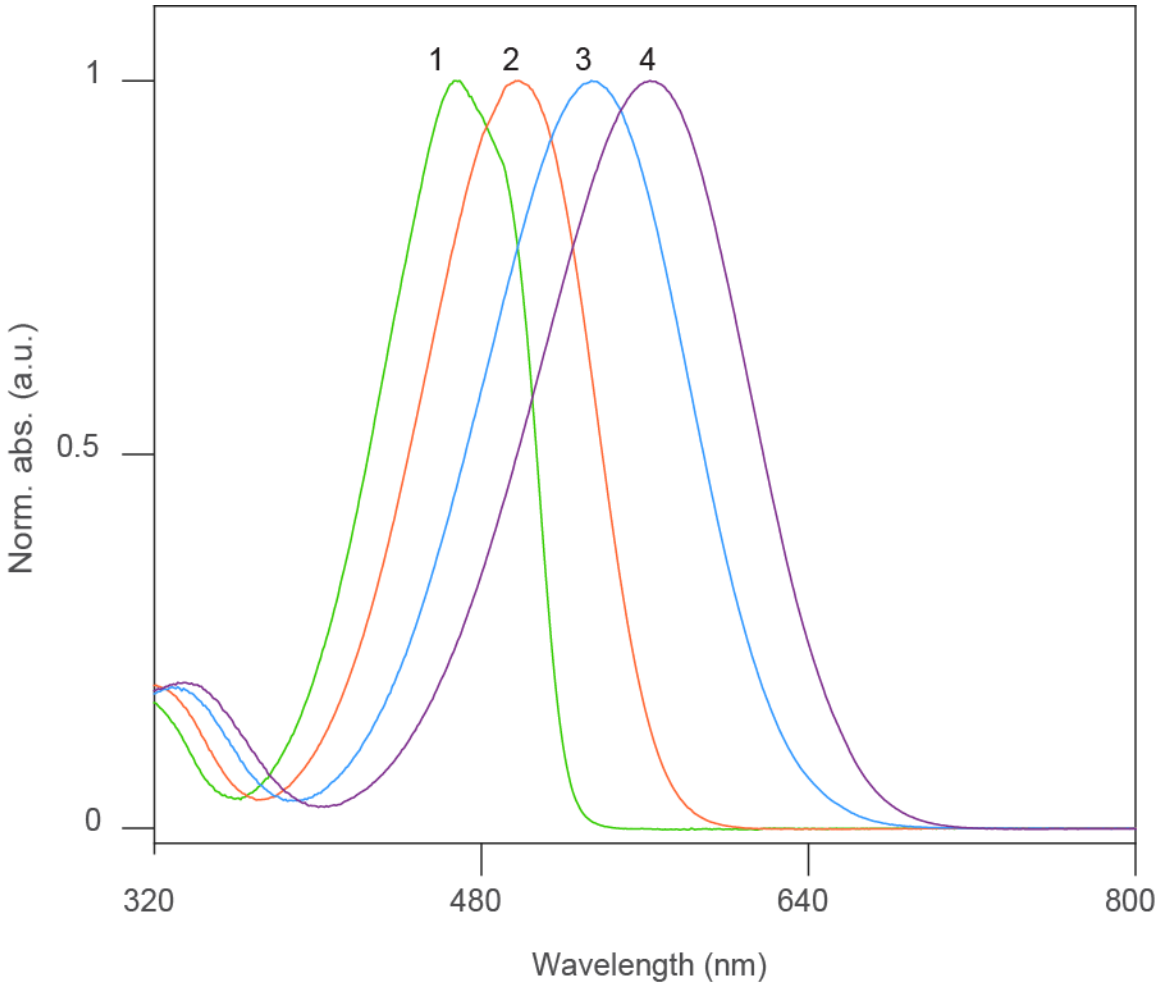

Figure 3.5 Solvachromism of **3** in (1) hexanes, (2) Et_2O, (3) CH_3CN, and (4) DMSO.

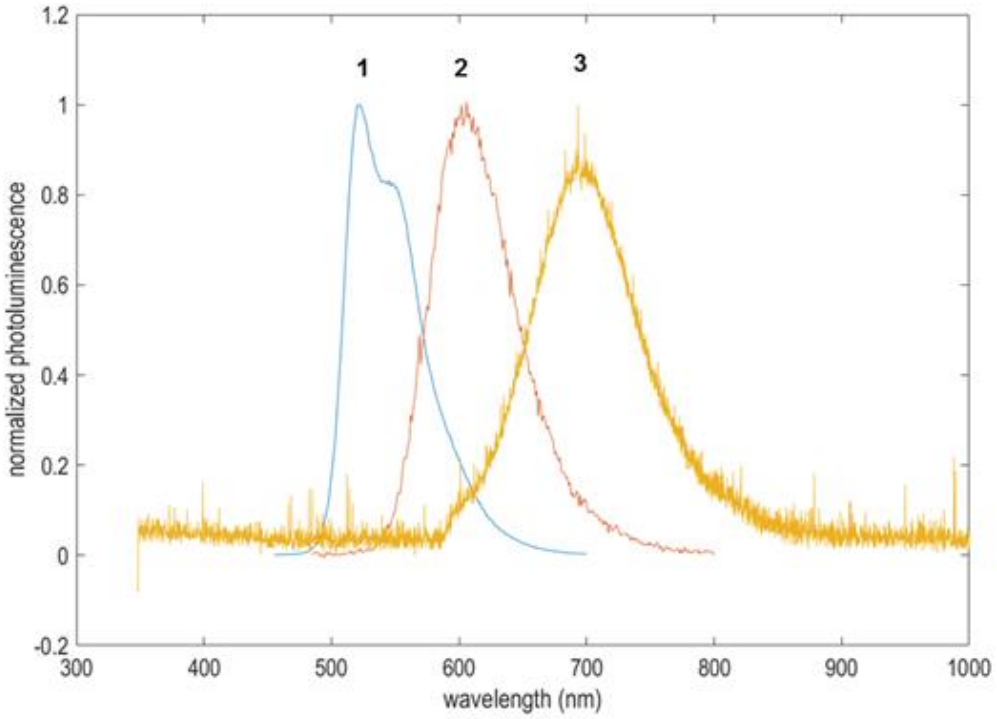

Figure 3.6 Photoluminescence (PL) spectra of dye **3** in various solvents displaying positive solvatochromism. (1) a solution of the dye in hexane (λ_{max} = 521 nm, excitation at 450 nm), (2) a solution of the dye in Et_2O (λ_{max} = 572 nm, excitation at 480 nm), and (3) a solution of the dye in DMSO (λ_{max} = 693 nm, excitation at 530-550). Note: PL spectrum of dye **3** in CH_3CN was also measured (excitation at 530), but the PL signal was not detected in our condition. The PL spectrum of the dye in DMSO was measured through a 590 nm long-pass filter.

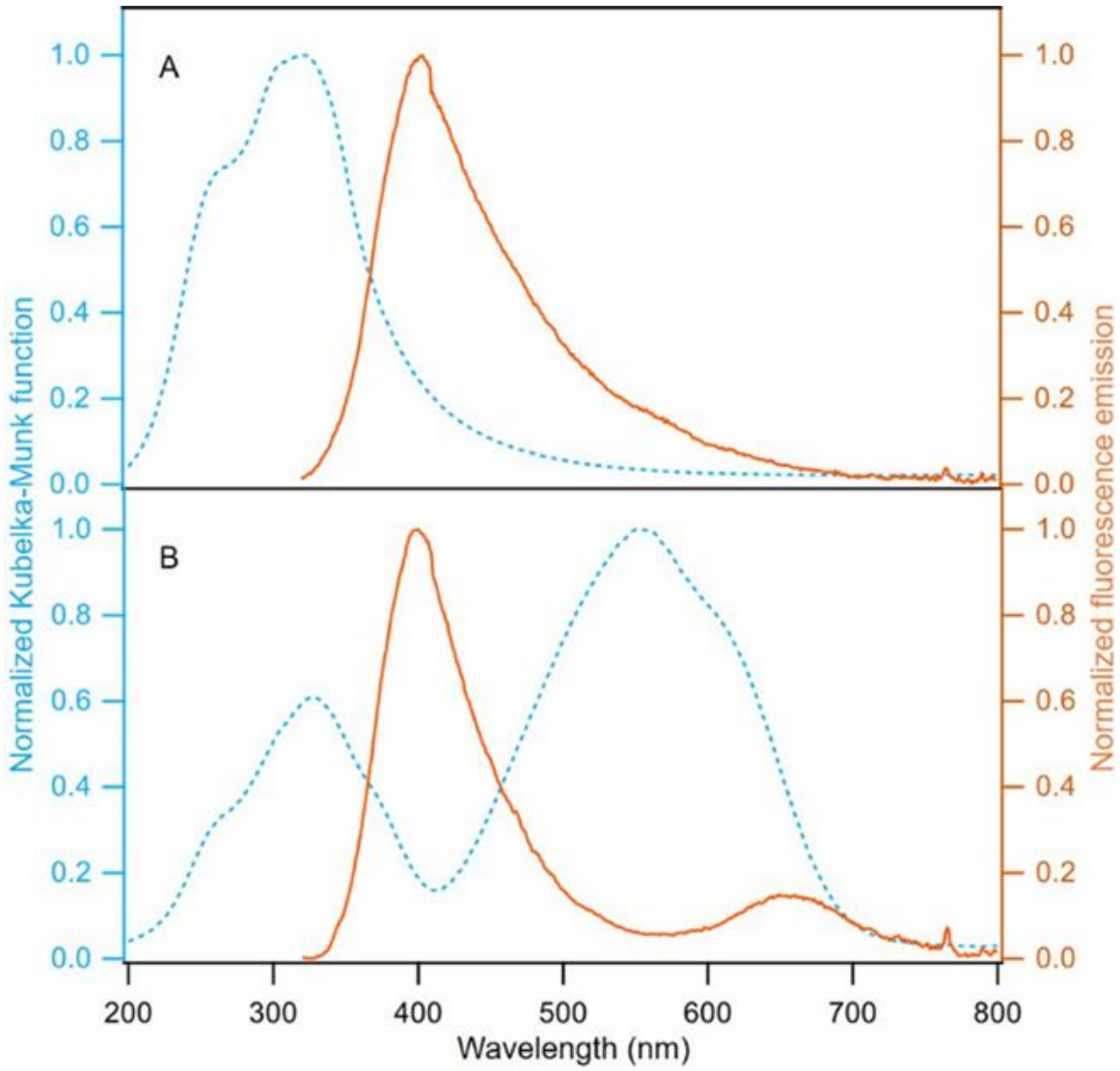

Figure 3.7 Diffuse reflectance spectra (dashed blue) and fluorescence emission spectra (solid orange) of (A) self-assembled phenylethynylene bis-urea macrocycle columnar structure **2** and (B) host–guest complex **4**.

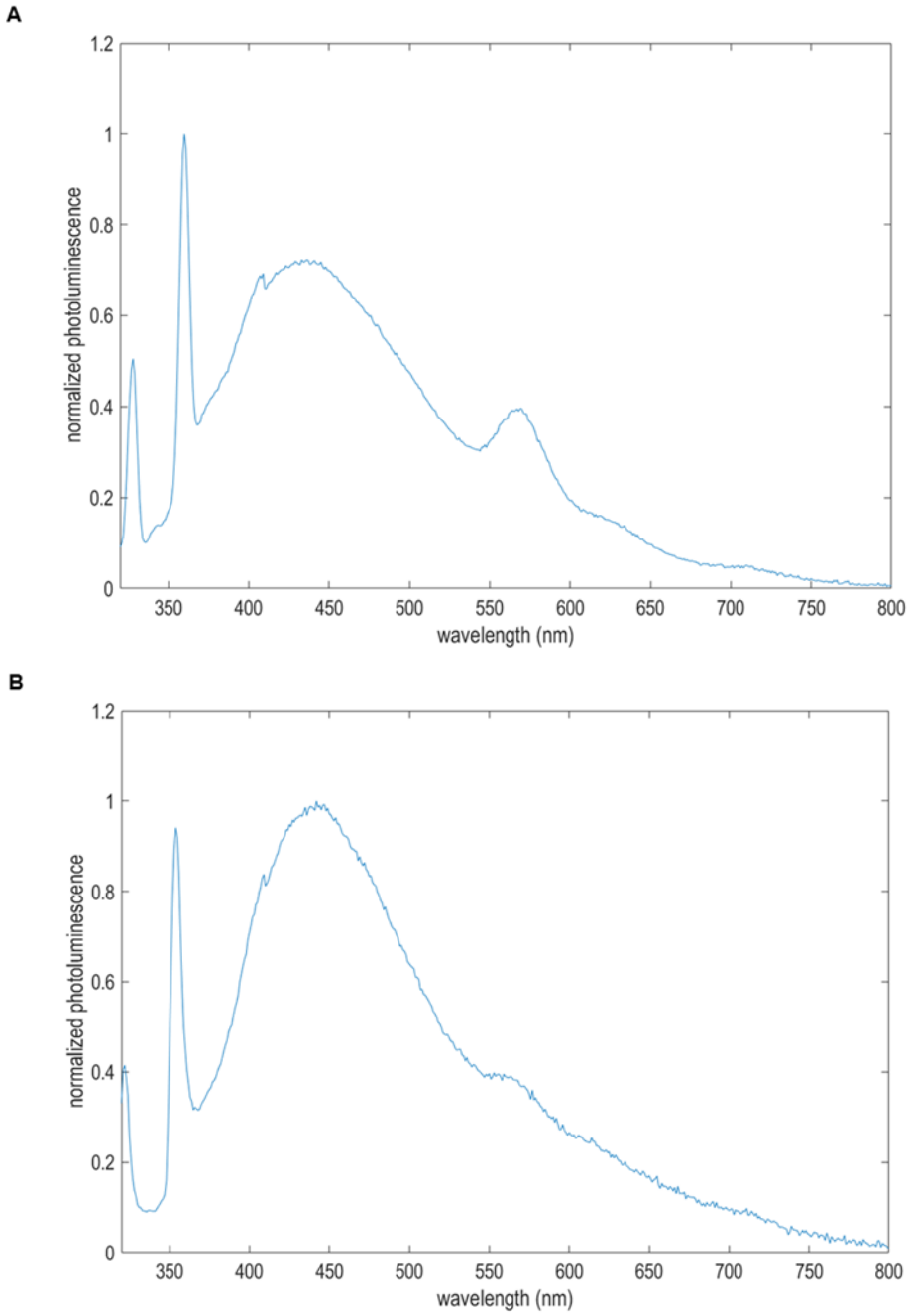

Figure 3.8 Solid-state photoluminescence spectra of (A) unactivated host fibers (excitation at 280 nm) and (B) unactivated host fibers treated with the solution of dye **3** (excitation at 280 nm). There is no peak at 649 nm attributed to the dye **3** as guest as appears in solid state photoluminescence spectra of the host-guest complex fibers **4** (Figure 3.7B). Note: the peaks at 360 nm and 328 nm in (A) and the peaks at 354 nm and 322 nm in (B) are caused by instrument-related artifacts; the peaks at 560 nm in both (A) and (B) are attributed to an artifact caused by 2nd order diffraction of excitation light.

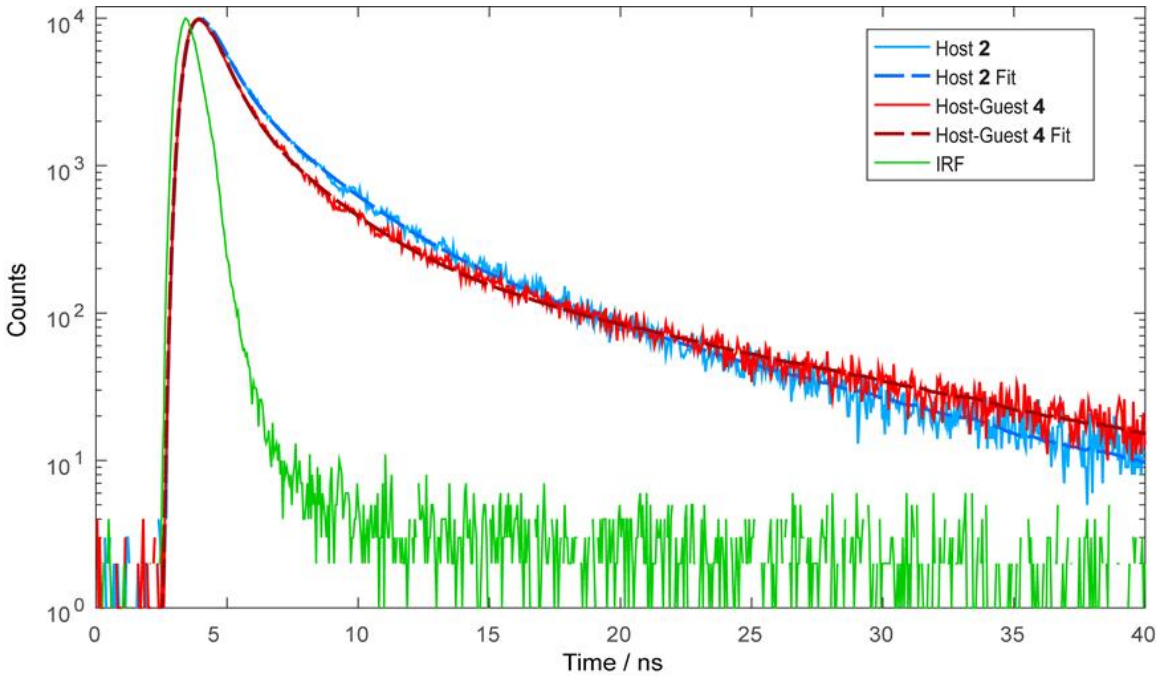

Figure 3.9 Fluorescence decays host **2** (blue), dye-treated host **2** (red) and green is IRF. Black solid lines are fits of the decays which were fitted with a triexponential function. The samples were excited at 300 nm. The emissions were measured through 430-475 nm band-pass filter.

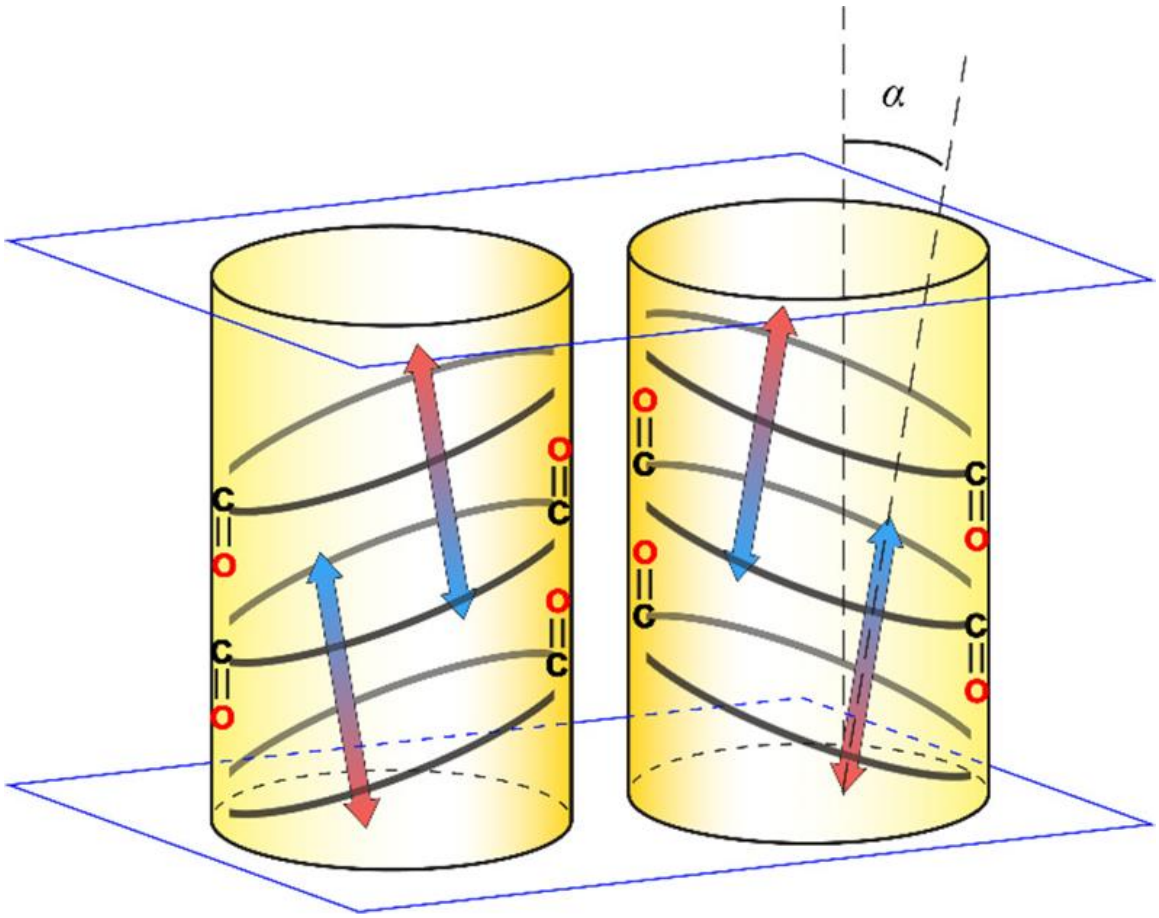

Figure 3.10 Four arrows illustrate four equivalent sites encompassing up and down orientations within the two 1D channels in the unit cell of **2**. Note that neighboring sites within a single channel are not simultaneously occupied based on the loading ratio measured for **4**. The complete X-ray structure of **2** is specified in ref 1, and the truncated model used in DFT calculations is illustrated in Figure 3.11.

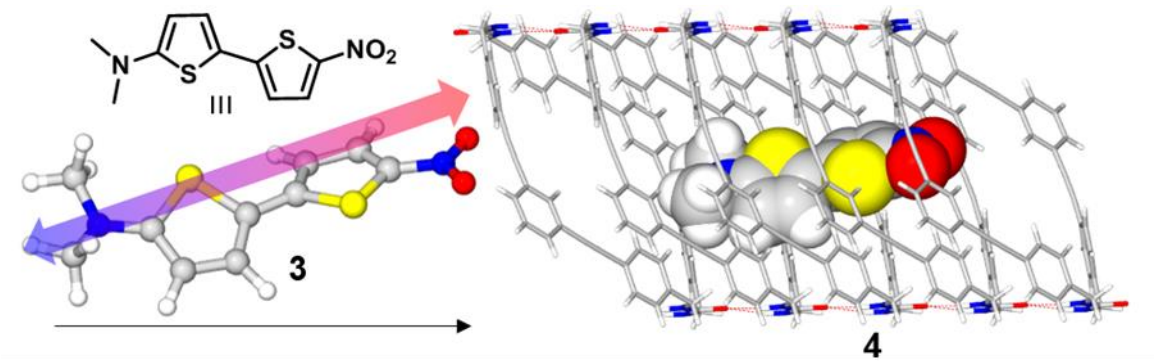

Figure 3.11 Optimized structure of 5-(dimethylamino)-5′-nitro-2,2′-bithiophene dye **3** and host–guest complex **4**. Arrow superimposed on **3** indicates electronic transition dipole moment (EDTM) orientation.

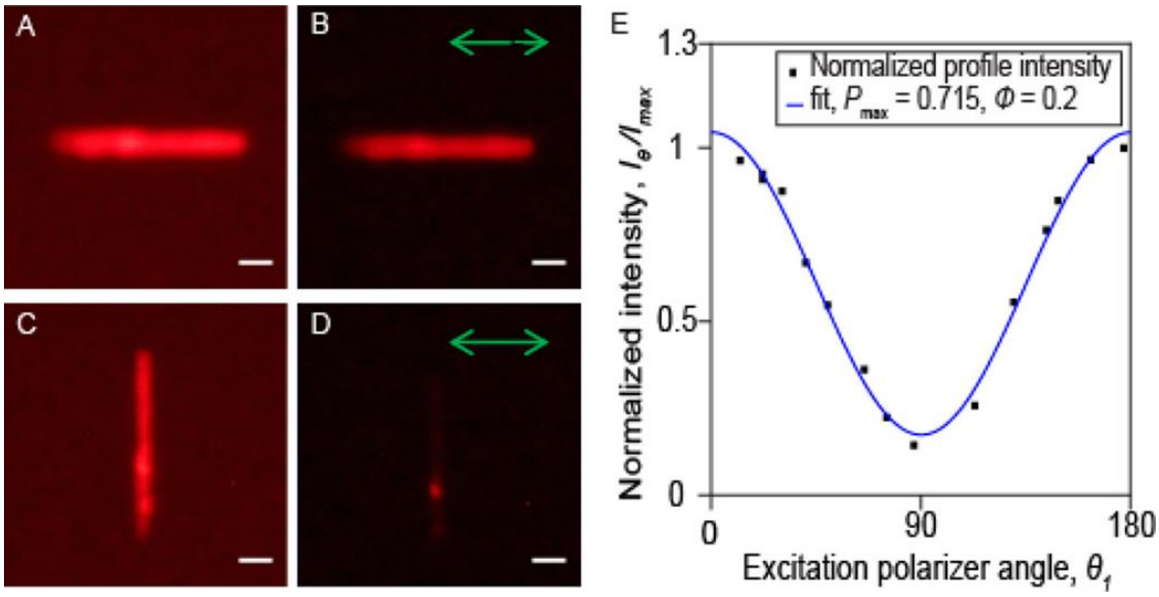

Figure 3.12 Excitation polarization measurement. (A–D) Micrographs of a single host–guest complex fiber recorded with varying excitation conditions (scale bars are 10 μm). Panels A and C were recorded with an unpolarized condition, while panels B and D were recorded with polarized excitation with orientation indicated by green arrows. (E) Plot of I_θ/I_{max} (determined from averaged line profiles; see Appendix A) versus θ_1, shown with least-squares fit to eq 3.2.

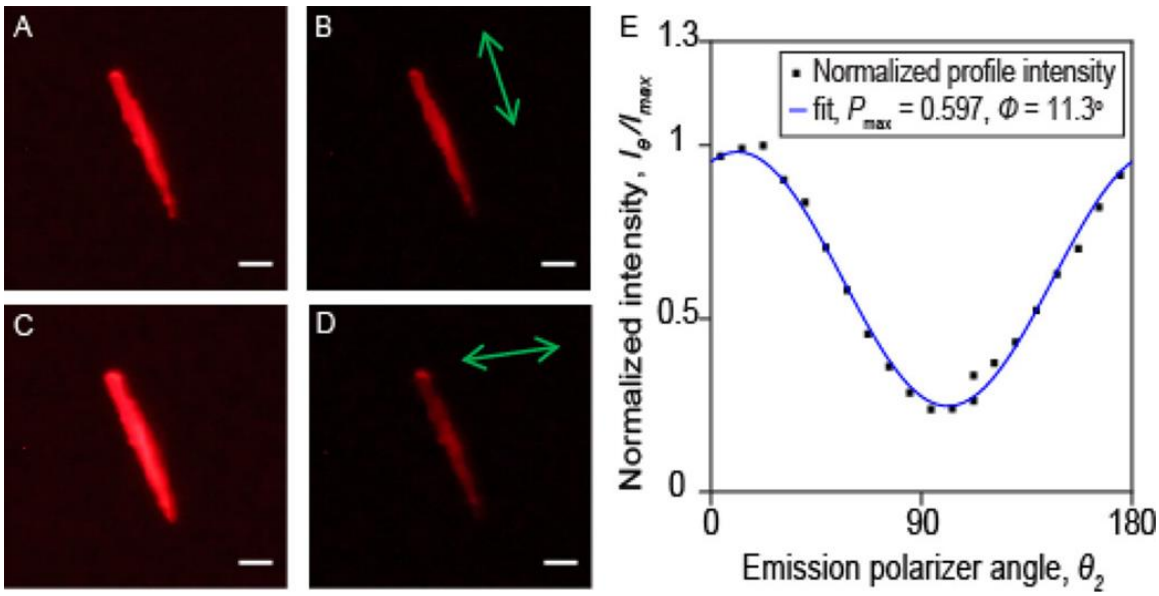

Figure 3.13 Emission polarization measurement. (A–D) Micrographs of a single host–guest complex fiber recorded with varying excitation conditions (scale bars are 10 μm). Panels A and C were recorded with an unpolarized condition, while panels B and D were recorded with polarized observation with orientation indicated by green arrows. (E) Plot of I_θ/I_{max} (determined from averaged line profiles; see Appendix A) versus θ_2, shown with least-squares fit to eq 3.2.

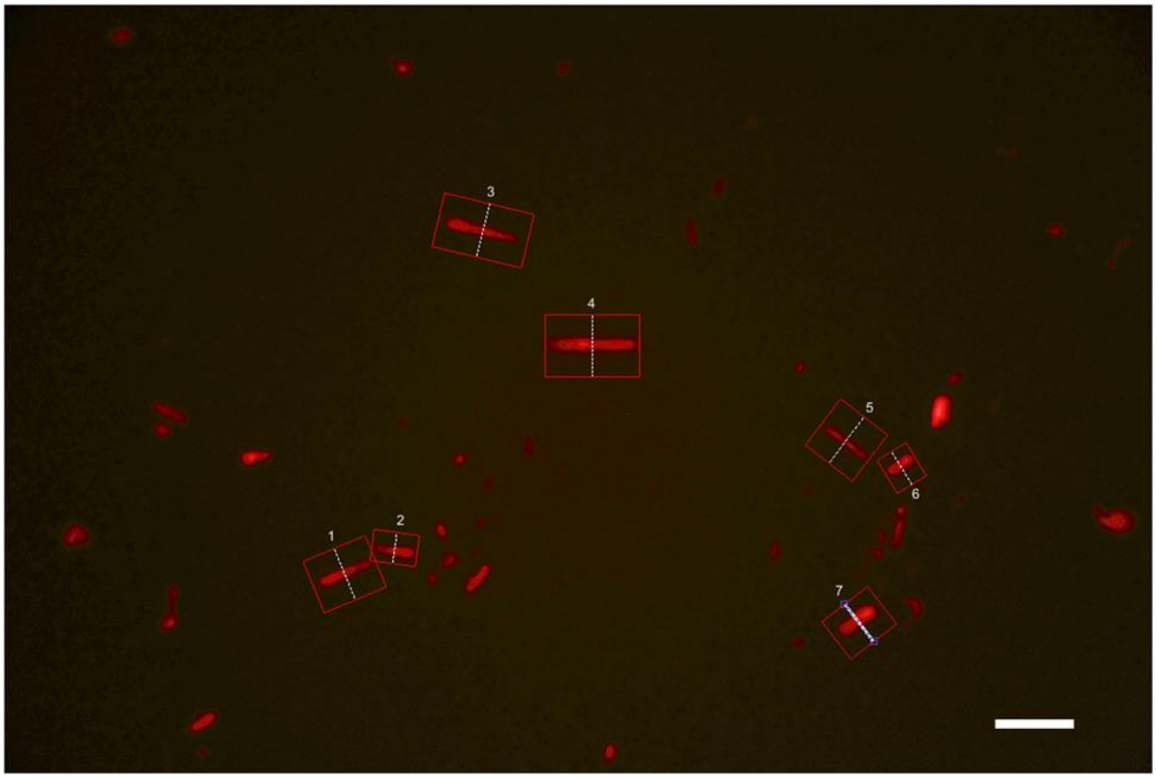

Figure 3.14 Fluorescence micrograph showing the host-guest complex fibers **4** used in excitation polarization anisotropy measurement excited with green excitation, scale bar: 50 µm. Each of the fibers is labelled with a profile number corresponding to the polarization anisotropy plots shown in Figure 3.15. The red rectangular boxes are regions of interest used for calculated fluorescence intensity of the fibers.

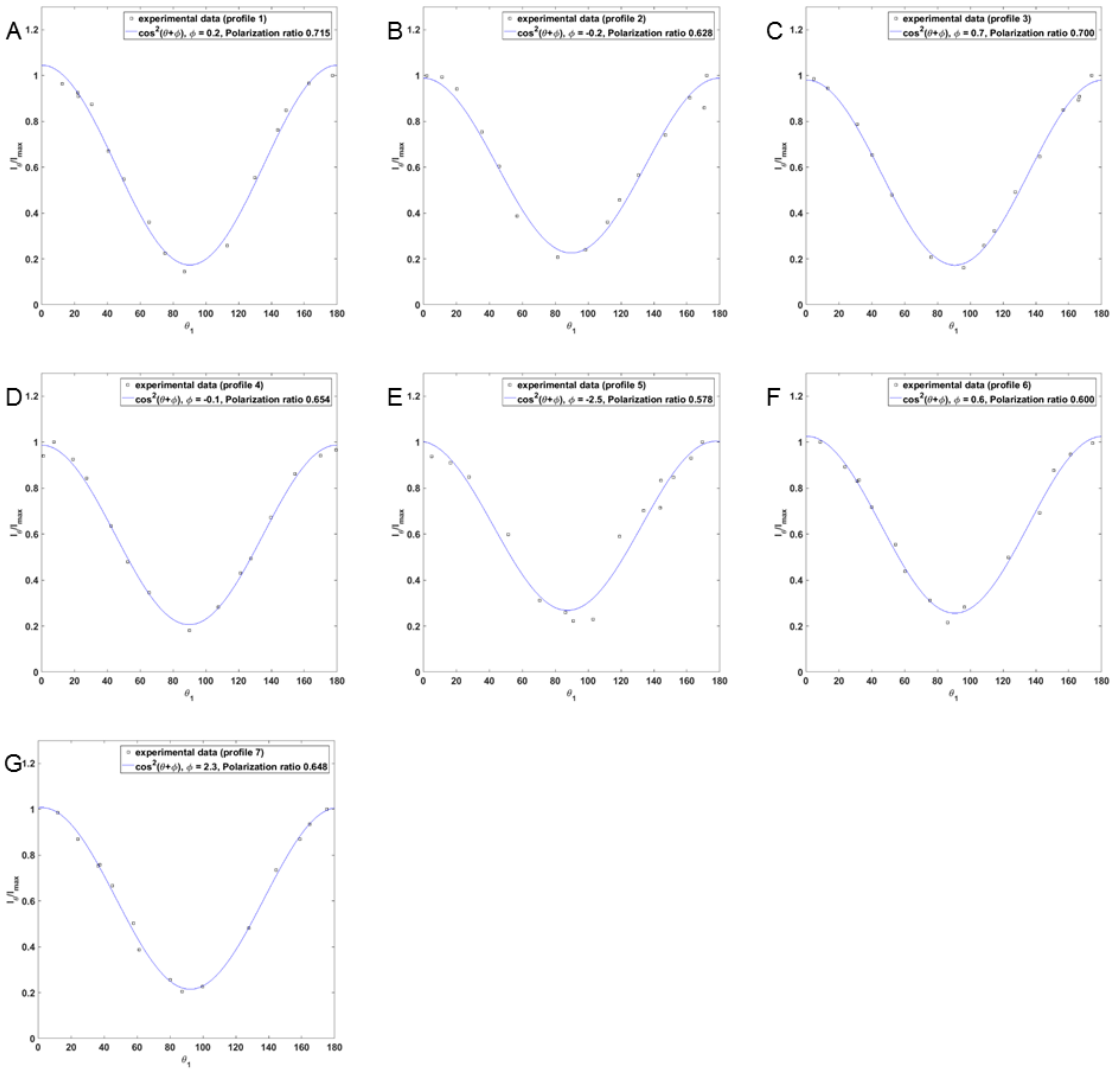

Figure 3.15 (A-G) Normalized intensity plots (analyzed from rgb channel) corresponding to profile 1-7 shown in Figure 3.14, respectively. The black squares show experimental data and the solid blue lines show $I_n + I_p \cos^2(\theta - \phi)$ function fitted to the experimental data. The polarization ratio is calculated from $I_p / (I_p + 2I_n)$.

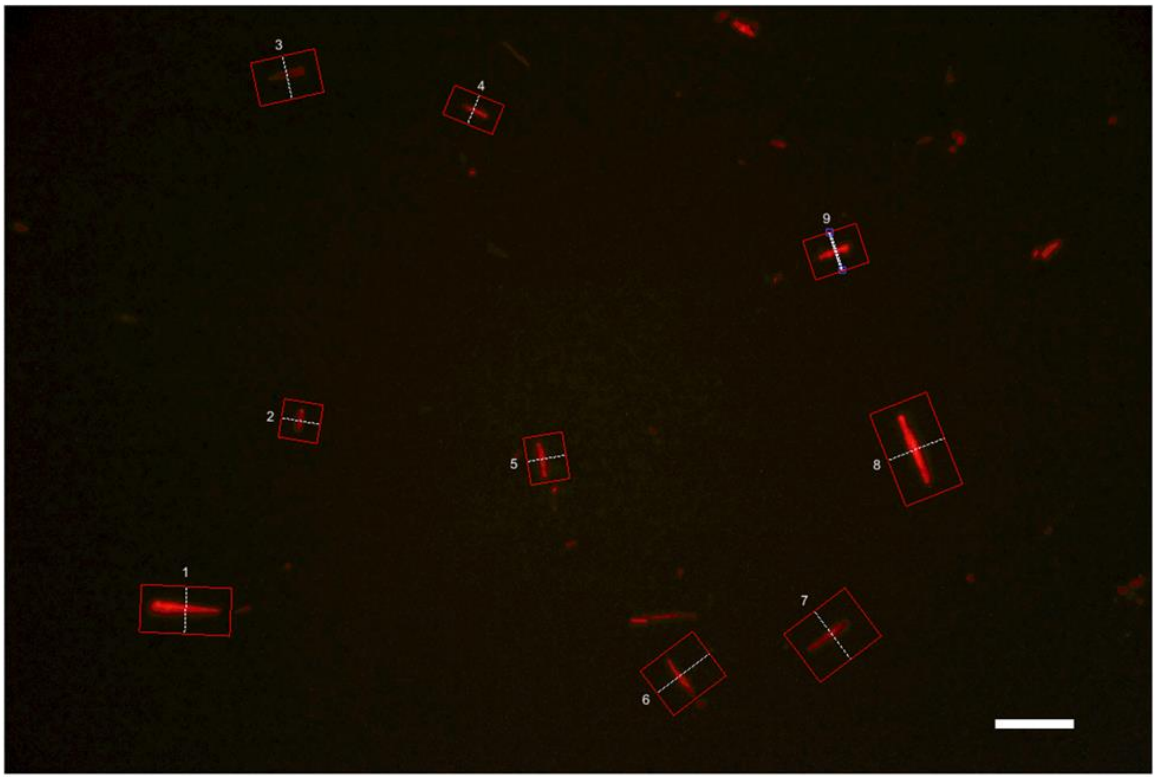

Figure 3.16 Fluorescence micrograph showing the host-guest complex fibers **4** used in emission polarization anisotropy measurement excited with green excitation, scale bar: 50 µm. Each of the fibers is labelled with a profile number corresponding to the polarization anisotropy plots shown in Figure 3.17. The red rectangular boxes are regions of interest used for calculated fluorescence intensity of the fibers.

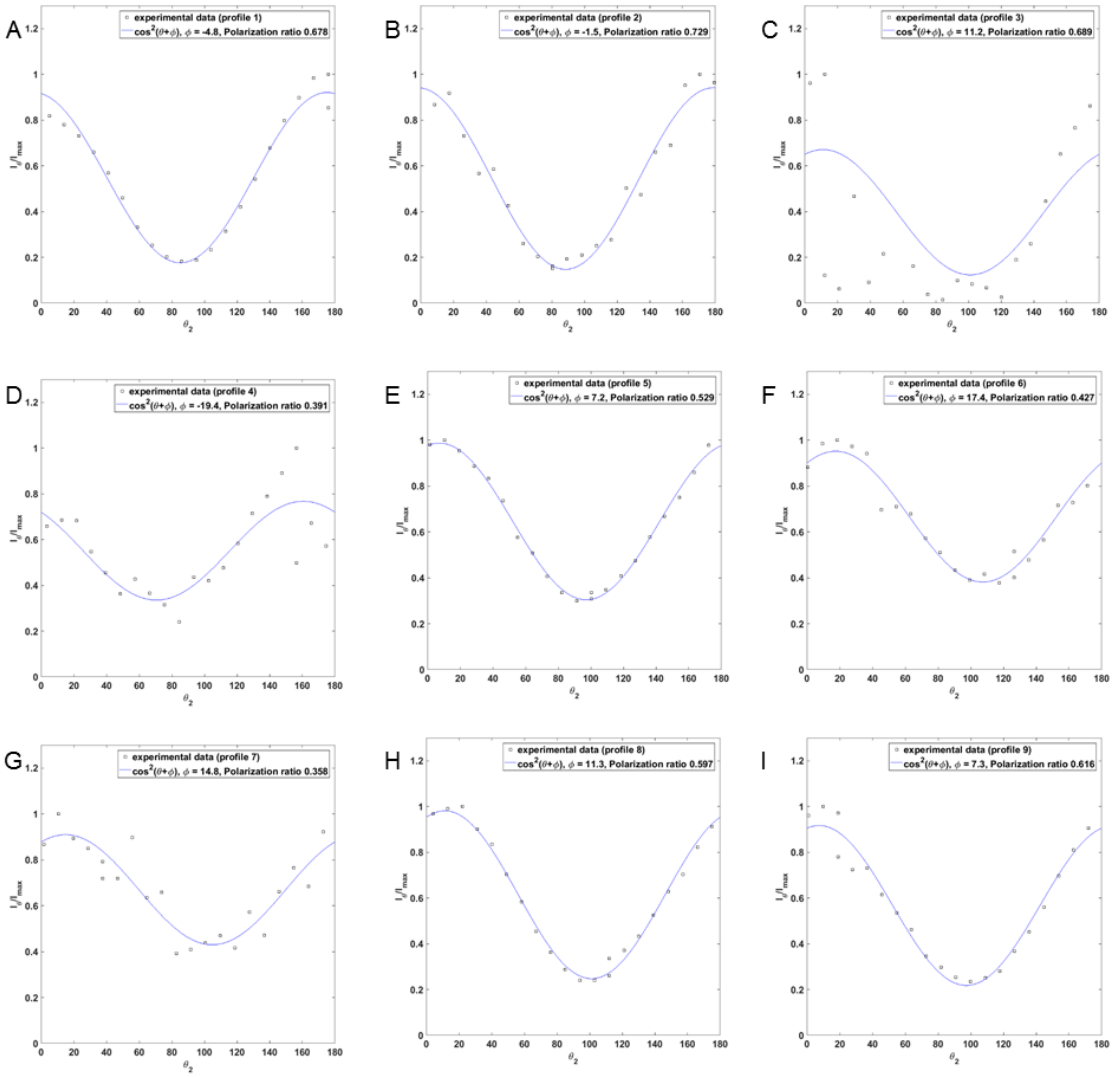

Figure 3.17 (A-I) Normalized intensity plots (analyzed from rgb channel) corresponding to profile 1-9 shown in Figure 3.16, respectively.

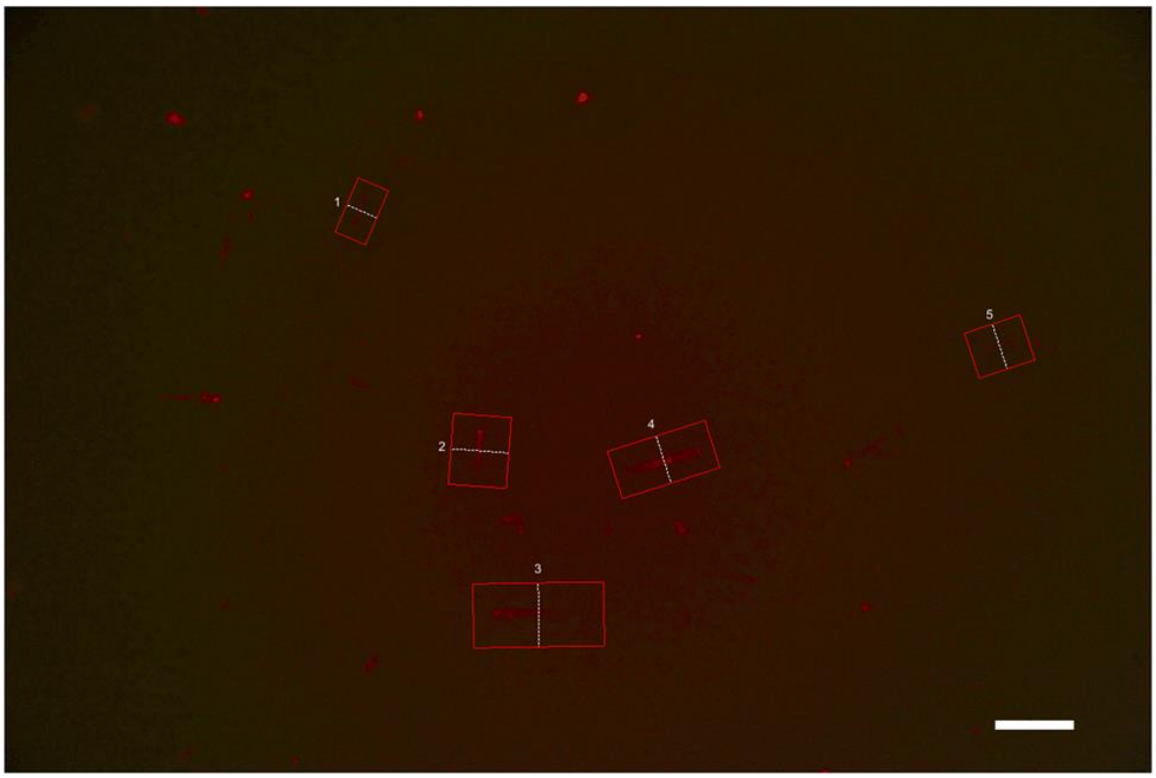

Figure 3.18 Fluorescence micrograph showing the dye-free host fibers **2** used in emission polarization anisotropy measurement excited with green excitation, scale bar: 50 µm. Each of the fibers is labelled with a profile number corresponding to the polarization anisotropy plots shown in Figure 3.19. The red rectangular boxes are regions of interest used for calculated fluorescence intensity of the fibers.

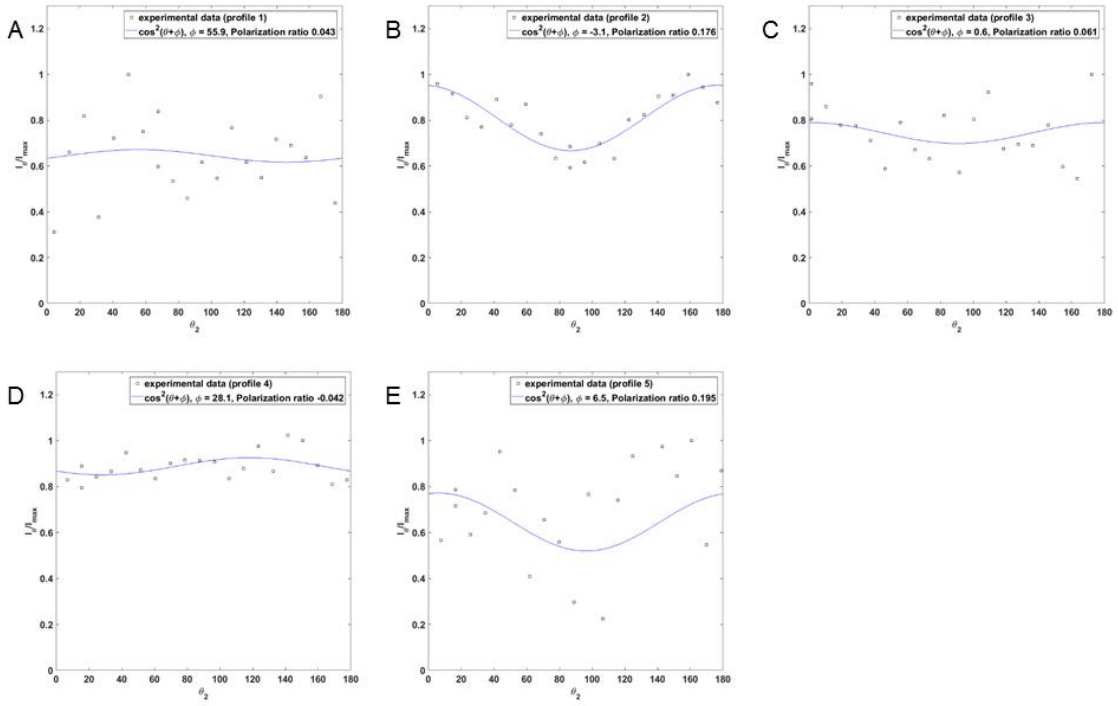

Figure 3.19 (A-E) Normalized intensity plots (analyzed from rgb channel) corresponding to profile 1-5 shown in Figure 3.18, respectively.

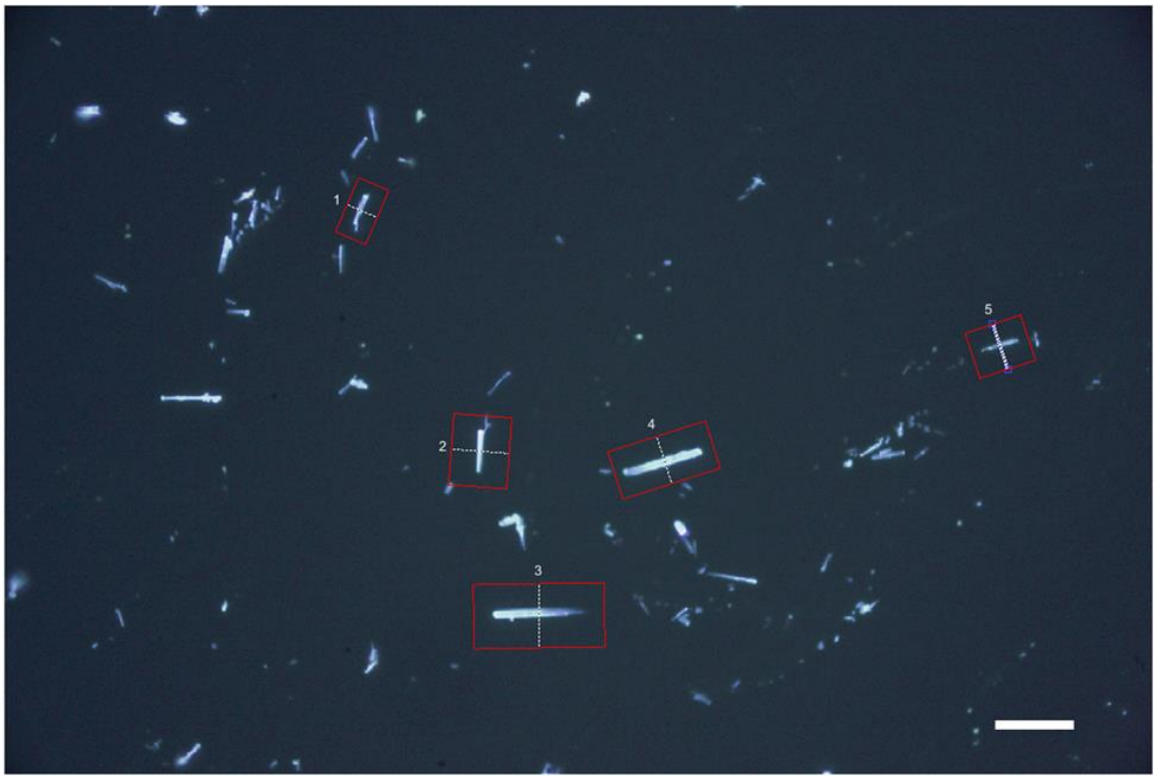

Figure 3.20 Fluorescence micrograph showing the dye-free host fibers **2** used in emission polarization anisotropy measurement excited with uv excitation, scale bar: 50 µm. Each of the fibers is labelled with a profile number corresponding to the polarization anisotropy plots shown in Figure 3.21. The red rectangular boxes are regions of interest used for calculated fluorescence intensity of the fibers.

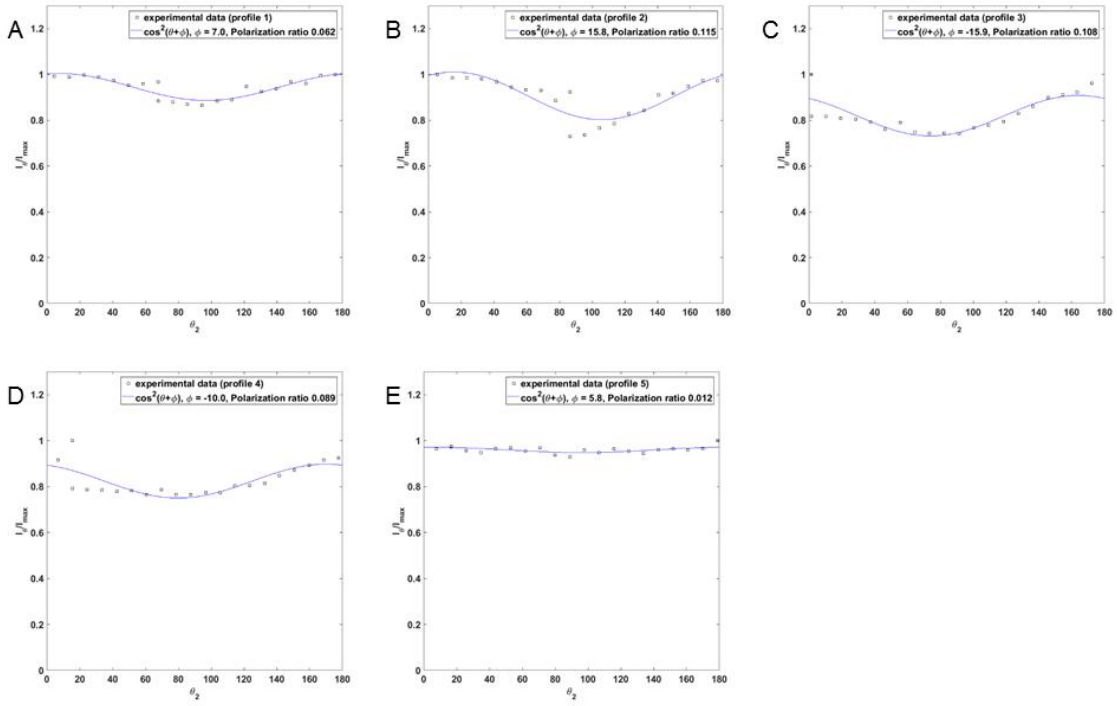

Figure 3.21 (A-E) Normalized intensity plots (analyzed from rgb channel) corresponding to profile 1-5 shown in Figure 3.20, respectively.

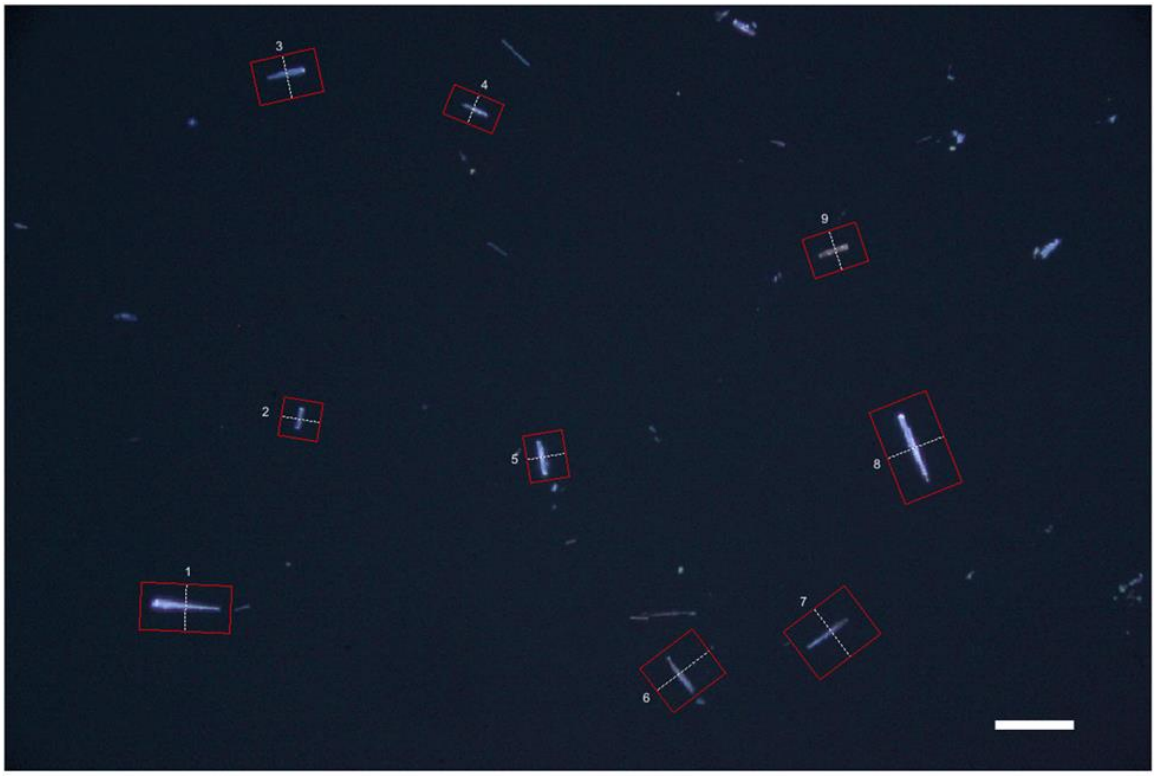

Figure 3.22 Fluorescence micrograph showing the host-guest complex fibers **4** used in emission polarization anisotropy measurement excited with UV excitation, scale bar: 50 μm. Each of the fibers is labelled with a profile number corresponding to the polarization anisotropy plots shown in Figure 3.23-3.25. The red rectangular boxes are regions of interest used for calculated fluorescence intensity of the fibers.

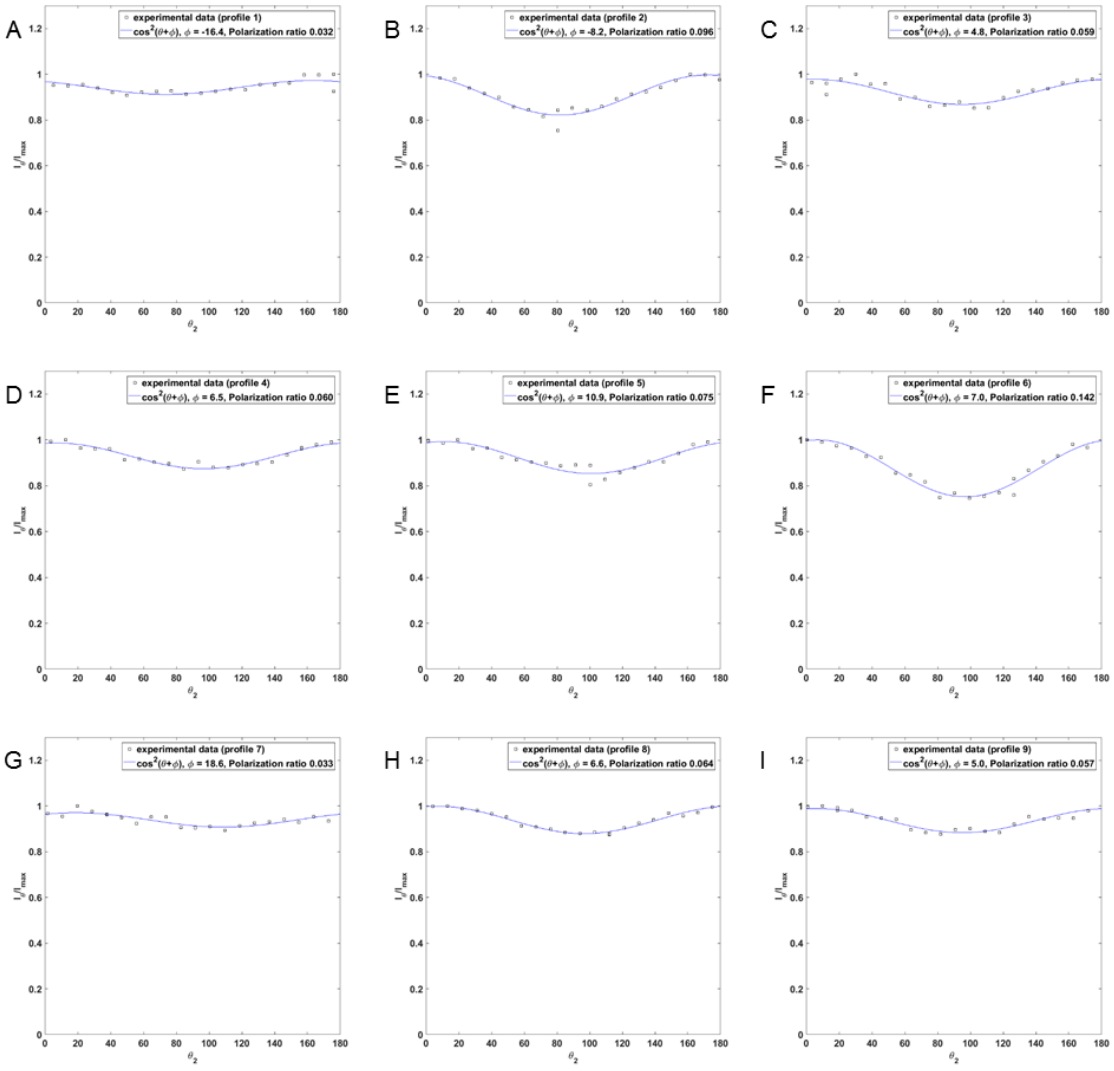

Figure 3.23 (A-I) Normalized intensity plots (analyzed from rgb channel) corresponding to profile 1-9 shown in Figure 3.22, respectively.

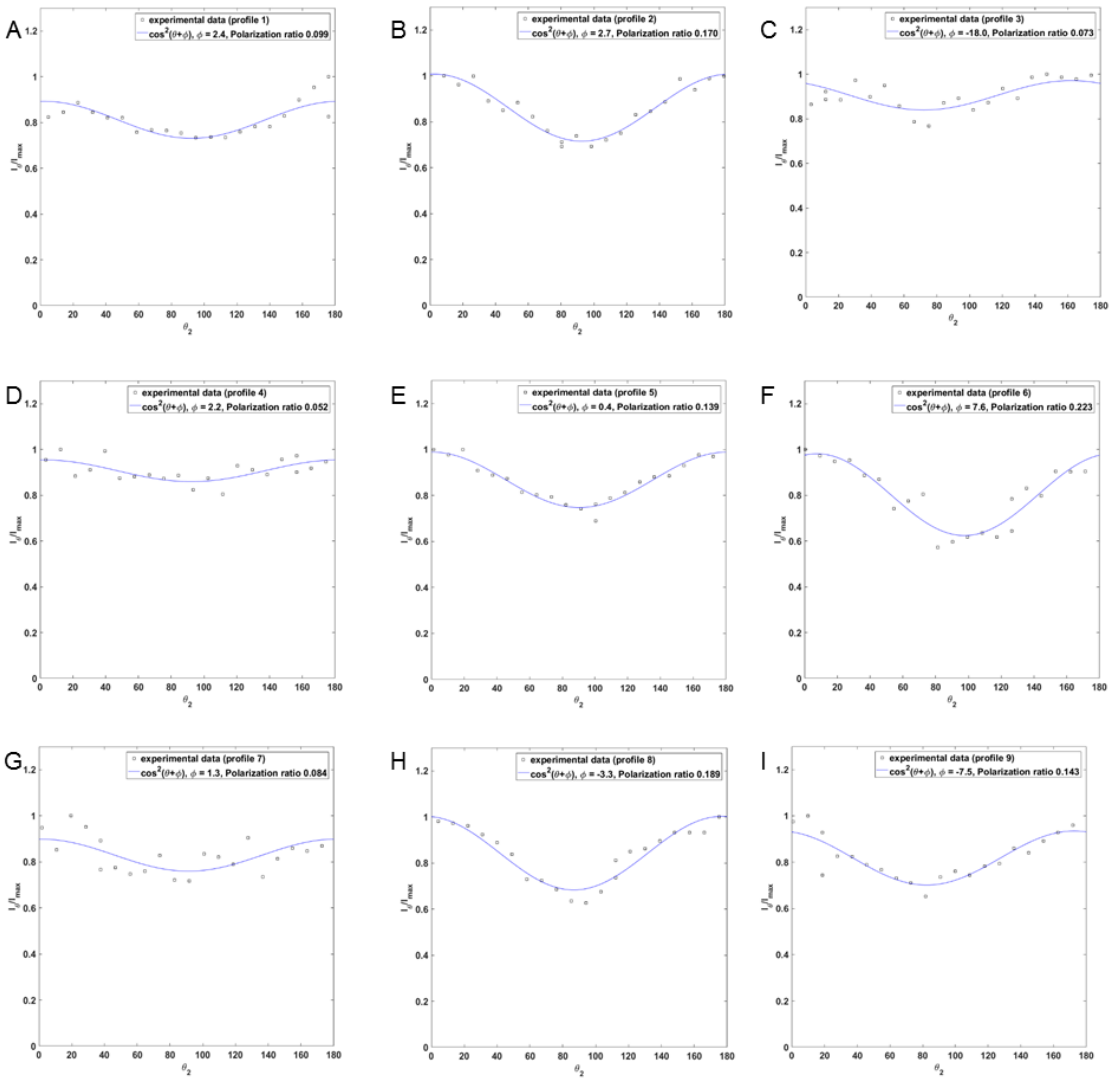

Figure 3.24 (A-I) Normalized intensity plots (analyzed from red channel) corresponding to profile 1-9 shown in Figure 3.22, respectively.

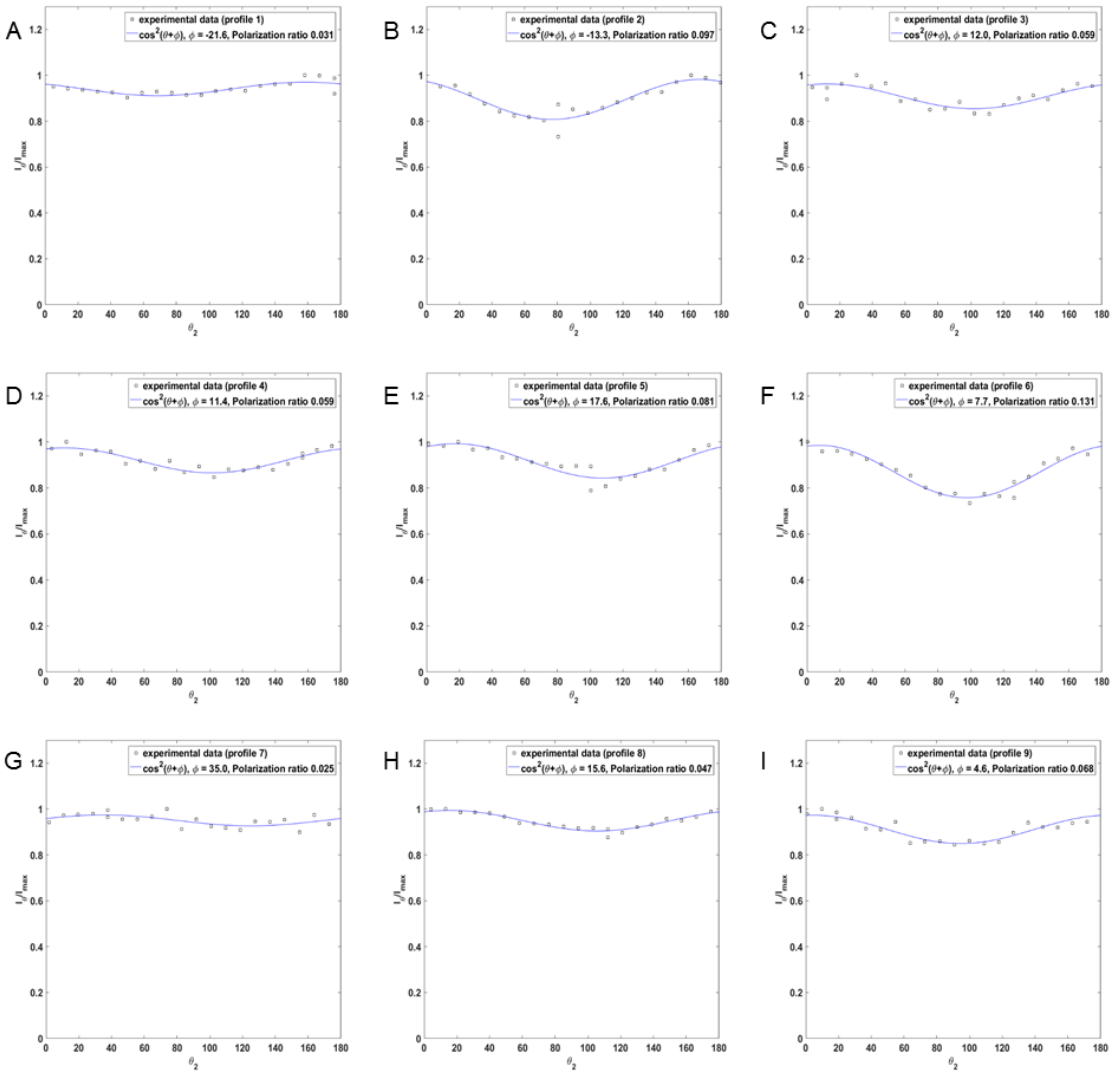

Figure 3.25 (A-I) Normalized intensity plots (analyzed from blue channel) corresponding to profile 1-9 shown in Figure 3.22, respectively.

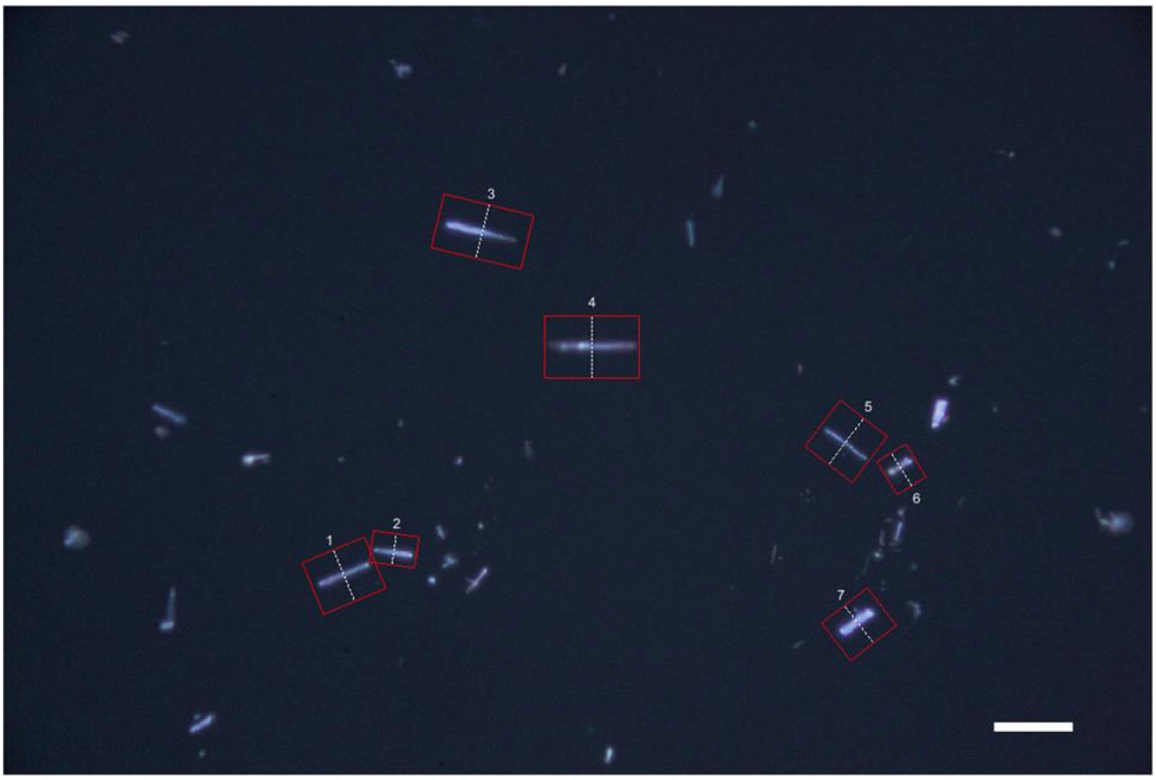

Figure 3.26 Fluorescence micrograph showing the host-guest complex fibers **4** used in excitation polarization anisotropy measurement excited with UV excitation, scale bar: 50 µm. Each of the fibers is labelled with a profile number corresponding to the polarization anisotropy plots shown in Figure 3.27. The red rectangular boxes are regions of interest used for calculated fluorescence intensity of the fibers.

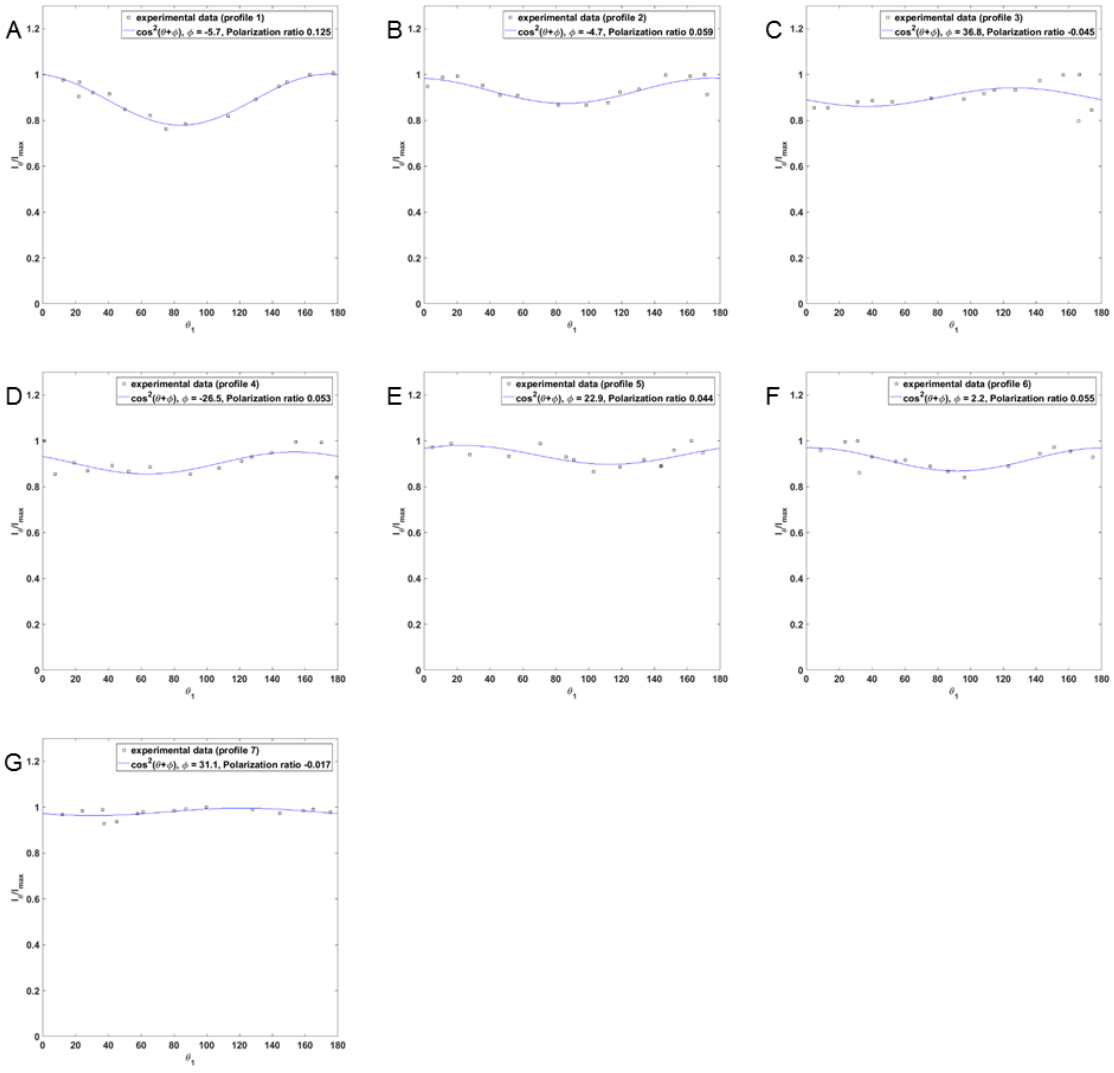

Figure 3.27 (A-G) Normalized intensity plots (analyzed from rgb channel) corresponding to profile 1-7 shown in Figure 3.26, respectively.

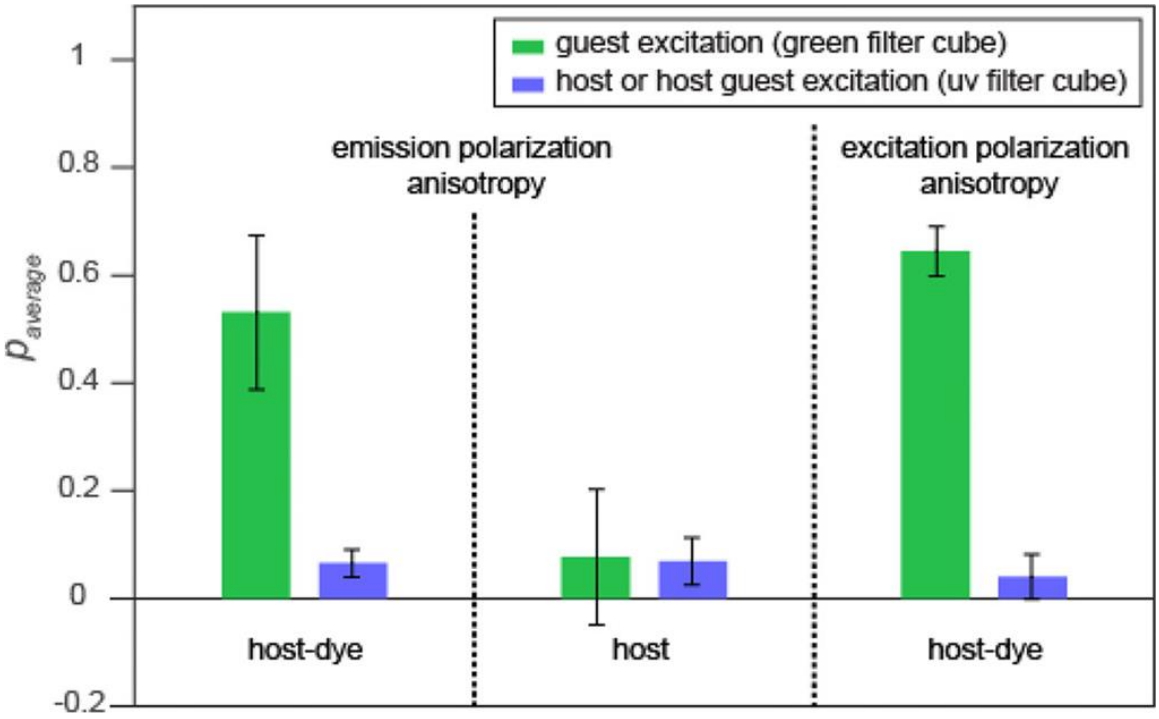

Figure 3.28 Average polarization, *P*, of the host–guest complex fibers **4** and host fibers **2** obtained from fluorescence emission polarization and fluorescence excitation polarization measurements under guest-selective visible excitation (green bars) or host/host–guest UV excitation (violet bars: data shown for total visible light fluorescence channel). Error bars indicate 95% confidence intervals. A complete summary of results is shown in Table 3.2.

CHAPTER 4
CONCLUSIONS[4]

We have shown here that the molecular fluorophore 5-(dimethylamino)-5′-nitro-2,2′-bithiophene **3** can be incorporated into self-assembled bis-urea macrocycle crystals containing 1D channels. Within the channels, the dye exhibits an absorbance peak position comparable to that seen in a highly polar solvent environment. Although **3** is almost nonfluorescent in such polar solvents, prominent fluorescence is observed in the context of the host matrix. Such enhancement of fluorescence in confined environments is also observed for the green fluorescent protein (GFP) chromophore, which is fluorescent in the protein and in metal–organic frameworks but nearly nonemissive in solution.[42] Polarized fluorescence microscopy measurements indicate that the ETDMs of the guests exhibit a net alignment parallel to the long axis of individual micrometer-scale crystals. A TDDFT calculation allows the EDTM to be indexed to the guest's molecular structure, and geometry optimization by DFT indicates that, while the minimized structure is tilted at ~9.5° from the channel axis, larger angles up to 30° are thermally accessible, which is sufficient to explain the maximum polarization values measured. Further studies of fluorescent guests with varied sizes or functional groups could aid in understanding and

[4] Kittikhunnatham, P.; Som, B.; Rassolov, V.; Stolte, M.; Würthner, F.; Shimizu, L. S.; Greytak A. B. Fluorescence polarization measurements to probe alignment of a bithiophene dye in one-dimensional channels of self-assembled phenylethynylene bis-urea macrocycle crystals. *J. Phys. Chem. C* **2017**, *121* (33), 18102–18109.
Reprinted here with permission of publisher.

modeling host–guest interactions in porous organic crystals. Due to its ability to detect molecular orientation information on single micro/nanoscale structures with low detection limit, polarized fluorescence microscopy can potentially be used to probe other types of low-dimensional porous materials. Furthermore, combining this technique with time-series image analysis should facilitate the study of kinetics and transport processes in such low-dimensional systems.

REFERENCES

(1) Dawn, S.; Dewal, M. B.; Sobransingh, D.; Paderes, M. C.; Wibowo, A. C.; Smith, M. D.; Krause, J. A.; Pellechia, P. J.; Shimizu, L. S. Self-Assembled Phenylethynylene Bis-Urea Macrocycles Facilitate the Selective Photodimerization of Coumarin. *J. Am. Chem. Soc.* **2011**, *133*, 7025–7032.

(2) Salpage, S. R.; Donevant, L. S.; Smith, M. D.; Bick, A.; Shimizu, L. S. Modulating the Reactivity of Chromone and Its Derivatives through Encapsulation in a Self-Assembled Phenylethynylene Bis-Urea Host. *J. Photochem. Photobiol. -Chem.* **2016**, *315*, 14–24.

(3) Geer, M. F.; Walla, M. D.; Solntsev, K. M.; Strassert, C. A.; Shimizu, L. S. Self-Assembled Benzophenone Bis-Urea Macrocycles Facilitate Selective Oxidations by Singlet Oxygen. *J. Org. Chem.* **2013**, *78*, 5568–5578.

(4) Calzaferri, G.; Pauchard, M.; Maas, H.; Huber, S.; Khatyr, A.; Schaafsma, T. Photonic Antenna System for Light Harvesting, Transport and Trapping. *J. Mater. Chem.* **2002**, *12*, 1–13.

(5) Calzaferri, G.; Huber, S.; Maas, H.; Minkowski, C. Host–guest Antenna Materials. *Angew. Chem. Int. Ed.* **2003**, *42*, 3732–3758.

(6) Calzaferri, G.; Lutkouskaya, K. Mimicking the Antenna System of Green Plants. *Photochem. Photobiol. Sci.* **2008**, *7*, 879–910.

(7) Calzaferri, G. Nanochannels: Hosts for the Supramolecular Organization of Molecules and Complexes. *Langmuir* **2012**, *28*, 6216–6231.

(8) Ramamurthy, V.; Sanderson, D. R.; Eaton, D. F. Control of Dye Assembly within Zeolites: Role of Water. *J. Am. Chem. Soc.* **1993**, *115*, 10438–10439.

(9) Meersmann, T.; Logan, J. W.; Simonutti, R.; Caldarelli, S.; Comotti, A.; Sozzani, P.; Kaiser, L. G.; Pines, A. Exploring Single-File Diffusion in One-Dimensional Nanochannels by Laser-Polarized 129Xe NMR Spectroscopy. *J. Phys. Chem. A* **2000**, *104*, 11665–11670.

(10) Sozzani, P.; Comotti, A.; Simonutti, R.; Meersmann, T.; Logan, J. W.; Pines, A. A Porous Crystalline Molecular Solid Explored by Hyperpolarized Xenon. *Angew. Chem. Int. Ed.* **2000**, *39*, 2695–2699.

(11) Langley, P. J.; Hulliger, J. Nanoporous and Mesoporous Organic Structures: New Openings for Materials Research. *Chem. Soc. Rev.* **1999**, *28*, 279–291.

(12) Couderc, G.; Hulliger, J. Channel Forming Organic Crystals: Guest Alignment and Properties. *Chem. Soc. Rev.* **2010**, *39*, 1545–1554.

(13) Bowers, C. R.; Dvoyashkin, M.; Salpage, S. R.; Akel, C.; Bhase, H.; Geer, M. F.; Shimizu, L. S. Crystalline Bis-Urea Nanochannel Architectures Tailored for Single-File Diffusion Studies. *Acs Nano* **2015**, *9*, 6343–6353.

(14) Swager, T. M. Iptycenes in the Design of High Performance Polymers. *Acc. Chem. Res.* **2008**, *41*, 1181–1189.

(15) Xu, W. L.; Smith, M. D.; Krause, J. A.; Greytak, A. B.; Ma, S.; Read, C. M.; Shimizu, L. S. Single Crystal to Single Crystal Polymerization of a Self-Assembled Diacetylene Macrocycle Affords Columnar Polydiacetylenes. *Cryst. Growth Des.* **2014**, *14*, 993–1002.

(16) Dawn, S.; Salpage, S. R.; Koscher, B. A.; Bick, A.; Wibowo, A. C.; Pellechia, P. J.; Shimizu, L. S. Applications of a Bis-Urea Phenylethynylene Self-Assembled Nanoreactor for [2+2] Photodimerizations. *J. Phys. Chem. A* **2014**, *118*, 10563–10574.

(17) Effenberger, F.; Würthner, F. 5-Dimethylamino-5′-Nitro-2, 2′-Bithiophene—a New Dye with Pronounced Positive Solvatochromism. *Angew. Chem. Int. Ed. Engl.* **1993**, *32*, 719–721.

(18) Effenberger, F.; Wuerthner, F.; Steybe, F. Synthesis and Solvatochromic Properties of Donor-Acceptor-Substituted Oligothiophenes. *J. Org. Chem.* **1995**, *60*, 2082–2091.

(19) Iwanaga, H.; Naito, K.; Effenberger, F. Oligothiophene Dyes for Guest-Host Liquid Crystal Displays. *Liq. Cryst.* **2000**, *27*, 115–123.

(20) Rodríguez-Méndez, M. L.; Apetrei, C.; Nieto, M.; Hernandez, V.; Navarrete, J. T. L.; Effenberger, F.; de Saja, J. A. Sensing Properties of Organised Films Based on a Bithiophene Derivative. *Sens. Actuators B Chem.* **2009**, *141*, 625–633.

(21) Gierschner, J. Directional Exciton Transport in Supramolecular Nanostructured Assemblies. *Phys. Chem. Chem. Phys.* **2012**, *14*, 13146–13153.

(22) Fois, E.; Tabacchi, G.; Calzaferri, G. Interactions, Behavior, and Stability of Fluorenone inside Zeolite Nanochannels. *J. Phys. Chem. C* **2010**, *114*, 10572–10579.

(23) Fois, E.; Tabacchi, G.; Calzaferri, G. Orientation and Order of Xanthene Dyes in the One-Dimensional Channels of Zeolite L: Bridging the Gap between Experimental Data and Molecular Behavior. *J. Phys. Chem. C* **2012**, *116*, 16784–16799.

(24) Fois, E.; Tabacchi, G.; Devaux, A.; Belser, P.; Brühwiler, D.; Calzaferri, G. Host–guest Interactions and Orientation of Dyes in the One-Dimensional Channels of Zeolite L. *Langmuir* **2013**, *29*, 9188–9198.

(25) Zhou, X.; Wesolowski, T. A.; Tabacchi, G.; Fois, E.; Calzaferri, G.; Devaux, A. First-Principles Simulation of the Absorption Bands of Fluorenone in Zeolite L. *Phys. Chem. Chem. Phys.* **2013**, *15*, 159–167.

(26) Srinivasan, G.; Villanueva-Garibay, J. A.; Müller, K.; Oelkrug, D.; Medina, B. M.; Beljonne, D.; Cornil, J.; Wykes, M.; Viani, L.; Gierschner, J.; et al. Dynamics of Guest Molecules in PHTP Inclusion Compounds as Probed by Solid-State NMR and Fluorescence Spectroscopy. *Phys. Chem. Chem. Phys.* **2009**, *11*, 4996–5009.

(27) Tsuwi, J.; Berger, R.; Labat, G.; Couderc, G.; Behrnd, N.-R.; Ottiger, P.; Cucinotta, F.; Schürmann, K.; Bertoni, M.; Viani, L.; et al. Alignment and Relaxation Dynamics of Dye Molecules in Host−Guest Inclusion Compounds As Probed by Dielectric Spectroscopy. *J. Phys. Chem. A* **2010**, *114*, 6956–6963.

(28) Lee, S. K.; Shang, Q.-Y.; Hudson, B. S. Urea and Thiourea Inclusion Complexes of Conjugated Polyenes: Polarized Fluorescence Excitation and Resonance Raman Studies. *Mol. Cryst. Liq. Cryst. Sci. Technol. Sect. Mol. Cryst. Liq. Cryst.* **1992**, *211*, 147–156.

(29) Gierschner, J.; Lüer, L.; Oelkrug, D.; Musluoğlu, E.; Behnisch, B.; Hanack, M. Preparation and Optical Properties of Oligophenylenevinylene/Perhydrotriphenylene Inclusion Compounds. *Adv. Mater.* **2000**, *12*, 757–761.

(30) Komorowska, K.; Brasselet, S.; Dutier, G.; Ledoux, I.; Zyss, J.; Poulsen, L.; Jazdzyk, M.; Egelhaaf, H.-J.; Gierschner, J.; Hanack, M. Nanometric Scale Investigation

of the Nonlinear Efficiency of Perhydrotriphenylene Inclusion Compounds. *Chem. Phys.* **2005**, *318*, 12–20.

(31) Huber, S.; Ruiz, A. Z.; Li, H.; Patrinoiu, G.; Botta, C.; Calzaferri, G. Optical Spectroscopy of Inorganic-Organic Host-Guest Nanocrystals Organized as Oriented Monolayers. *Inorganica Chim. Acta* **2007**, *360*, 869–875.

(32) Gasecka, A.; Dieu, L. Q.; Brühwiler, D.; Brasselet, S. Probing Molecular Order in Zeolite L Inclusion Compounds Using Two-Photon Fluorescence Polarimetric Microscopy. *J. Phys. Chem. B* **2010**, *114*, 4192–4198.

(33) Megelski, S.; Lieb, A.; Pauchard, M.; Drechsler, A.; Glaus, S.; Debus, C.; Meixner, A. J.; Calzaferri, G. Orientation of Fluorescent Dyes in the Nano Channels of Zeolite L. *J. Phys. Chem. B* **2001**, *105*, 25–35.

(34) Wu, J.; Gross, A. F.; Tolbert, S. H. Host-Guest Chemistry Using an Oriented Mesoporous Host: Alignment and Isolation of a Semiconducting Polymer in the Nanopores of an Ordered Silica Matrix. *J. Phys. Chem. B* **1999**, *103*, 2374–2384.

(35) Kampmann, M.; Atkinson, C. E.; Mattheyses, A. L.; Simon, S. M. Mapping the Orientation of Nuclear Pore Proteins in Living Cells with Polarized Fluorescence Microscopy. *Nat. Struct. Mol. Biol.* **2011**, *18*, 643–649.

(36) Wang, J. F.; Gudiksen, M. S.; Duan, X. F.; Cui, Y.; Lieber, C. M. Highly Polarized Photoluminescence and Photodetection from Single Indium Phosphide Nanowires. *Science* **2001**, *293*, 1455–1457.

(37) Viswanath, A.; Paudel, P.; Kittikhunnatham, P.; Green, A. N.; Greytak, A. B.; Benicewicz, B. C. Synthesis of Random Terpolymers Bearing Multidentate Imidazole

Units and Their Use in Functionalization of Cadmium Sulfide Nanowires. *Polym. Chem.* **2015**, *6*, 7036–7044.

(38) Kamlet, M. J.; Abboud, J. L.; Taft, R. W. The Solvatochromic Comparison Method. 6. The Pi.* Scale of Solvent Polarities. *J. Am. Chem. Soc.* **1977**, *99*, 6027–6038.

(39) Kamlet, M. J.; Abboud, J. L. M.; Abraham, M. H.; Taft, R. W. Linear Solvation Energy Relationships. 23. A Comprehensive Collection of the Solvatochromic Parameters, Pi.*, .Alpha., and .Beta., and Some Methods for Simplifying the Generalized Solvatochromic Equation. *J. Org. Chem.* **1983**, *48*, 2877–2887.

(40) Sillen, A.; Engelborghs, Y. The Correct Use of "Average" Fluorescence Parameters. *Photochem. Photobiol.* **1998**, *67*, 475–486.

(41) te Velde, G.; Bickelhaupt, F. M.; Baerends, E. J.; Fonseca Guerra, C.; van Gisbergen, S. J. A.; Snijders, J. G.; Ziegler, T. Chemistry with ADF. *J. Comput. Chem.* **2001**, *22*, 931–967.

(42) Lakowicz, J. R. *Principles of Fluorescence Spectroscopy*, 3rd ed.; Springer: New York, 2006.

(43) Sillen, A.; Engelborghs, Y. The Correct Use of "Average" Fluorescence Parameters. Photochemistry and Photobiology 1998, 67, 475–486.

(44) Lipari, G.; Szabo, A. Effect of Librational Motion on Fluorescence Depolarization and Nuclear Magnetic Resonance Relaxation in Macromolecules and Membranes. Biophysical Journal 1980, 30, 489–506.

APPENDIX A

STATISTICAL INTERPRETATION OF POLARIZATION MEASUREMENTS

Detecting and quantifying polarization: We presume that when observed through the microscope objective, the light emitted by each individual crystal can be described as the sum of an unpolarized "normal" component with intensity I_n, and a component with intensity I_p that is linearly polarized. In general, the polarization axis of I_p may be displaced from the long axis of the crystal by an angle ϕ. If the fluorescence is associated with transition dipoles that are preferentially oriented along the crystal axis, we expect I_p to be non-zero, and ϕ to be small and centered about zero. The goal of this discussion is to establish conditions by which we can show that among the population of crystals in a sample, I_p is nonzero and ϕ is distributed non-randomly. We will show that these conditions can be established by demonstrating that the average polarization P among crystals in the sample, defined with respect to the crystal axis, is nonzero.

The polarization P of a beam of light can be defined as[43]

$$P = \frac{I_{\parallel} - I_{\perp}}{I_{\parallel} + I_{\perp}}$$

where $I_{\parallel}$ and $I_{\perp}$ represent the intensity measured with the excitation (or emission) polarizer oriented parallel or perpendicular to an axis of reference, taken here to be the crystal axis. Our measurement records the relative intensity I/I_{max} at a series of different angles θ between the polarizer and the crystal axis: $I_{\parallel}$ represents θ=0° and $I_{\perp}$ represents θ=90°. The

relative intensity, arising from the contributions of numerous individual transition dipoles within the sample, is expected to vary sinusoidally with θ, with a period of 180°:

$$I/I_{max} = I_n + I_p \cos^2(\theta - \phi)$$

Here, the maximum intensity, given by I_n+I_p, will be observed when $\theta=\phi$; the minimum intensity, given by I_n, when $\theta-\phi=90°$. ; and the average intensity $I_0=I_n+\frac{1}{2}I_p$. From this expression, we see that

$$I_{\parallel} = I_n+I_p \cos^2(-\phi) = I_n + I_p \cos^2\phi$$

$$I_{\perp} = I_n+I_p \cos^2(90°-\phi) = I_n + I_p(1-\cos^2\phi)$$

Substituting these into the expression for P above gives

$$P = \frac{I_p}{I_p + 2I_n}\cos 2\phi$$

Here, it can be seen that $I_p/(I_p+2I_n)$, which we refer to as P_{max}, is a positive number that is characteristic of the amplitude of oscillation and is equal to the maximum value of the polarization P (i.e. if it were measured with respect to the transition dipole such that ϕ = 0).

Values for P_{max} and ϕ can be obtained from a least-squares fit of I/I_{max} data. However, in the absence of any actual polarization, there are likely to be fluctuations in intensity among the data points that lead to a non-zero fit value for P_{max}, with random ϕ. It can be seen that regardless of the distribution of P_{max} values, the polarization $P = P_{max} \cos 2\phi$ will average to zero in a sample with randomly-oriented polarization angles ϕ. Thus, for each crystal, the polarization P is reconstructed from the fit values of P_{max} and ϕ. The average and sample standard deviation of P for all crystals observed is computed, and a confidence limit is established using a two-tailed t test with the number of degrees of freedom set as one less than the number of crystals examined, in recognition of the single parameter P.

Disorder in transition dipole orientations: The maximum polarization P_{max} observed for single fibers will be diminished in the case of disorder in EDTM of the fluorophores. Simple distributions that can be compared with experiment include static dipoles distributed symmetrically about the axis at a uniform angle (hollow cone); static dipoles distributed evenly over a spherical section within a characteristic angle (static cone); and dipoles that experience rotational diffusion over a spherical section within the decay lifetime (wobble in cone).[4] The use of unpolarized emission and detection channels in our experiment requires a modified approach from those used previously to analyze in conical distributions of fluorophores, e.g. in randomly oriented micelles.

We consider the case of an ensemble of molecules, with co-linear excitation and emission dipoles, whose distribution is described by a probability density $n(\alpha,\omega)$, where α is the tilt angle away from the channel axis (z direction) and ω is an azimuthal angle. Upon illumination, the distribution $f(\alpha,\omega)$ of excited dipoles is given by

$$f(\alpha,\omega)=(Ex_{\parallel}\cos^2\alpha+Ex_{\perp}\sin^2\alpha\sin^2\omega)\,n(\alpha,\omega)$$

where $Ex_{\parallel}$ represents the excitation power parallel to the axis and $Ex_{\perp}$ the power perpendicular. For an excitation polarization measurement, the selected polarization is 1 while the other is 0. For an emission polarization experiment, $Ex_{\parallel} = Ex_{\perp} = 1$.

The distribution of excited state fluorophores can then be integrated to obtain values proportional to the parallel and perpendicular polarization components of the light emitted by the sample:

$$Em_{\parallel}=\int_0^{\pi/2}d\alpha\int_0^{2\pi}\sin\alpha\;d\omega\;f(\alpha,\omega)\cos^2\alpha$$

$$Em_{\perp}=\int_0^{\pi/2}d\alpha\int_0^{2\pi}\sin\alpha\;d\omega\;f(\alpha,\omega)\sin^2\alpha\sin^2\omega$$

For an excitation polarization measurement, these components are added together to obtain the total intensity emitted under each excitation condition. For an emission polarization experiment, the two emitted components can be plugged in directly for $I_{\parallel}$ and $I_{\perp}$ to obtain the polarization. The integrals were solved numerically for the current analysis.

In the case of dynamic disorder (rotational diffusion), the excited state population $f(\alpha,\omega)$ can be allowed to evolve before the emitted light intensities are calculated. In the limit of complete relaxation, $f(\alpha,\omega)$ can be simply replaced with the static (equilibrium) distribution, but scaled according to the total amount of excitation that was achieved under parallel or perpendicular excitation:

$$f_{\infty}(\alpha,\omega) = n(\alpha,\omega) \times \frac{\iint f(\alpha,\omega)}{\iint n(\alpha,\omega)}$$

This description of the polarization neglects trivial causes of depolarization that include common-mode background contributions from host fluorescence and attenuation or scattering of excitation or emission light within the crystals or at their boundaries.

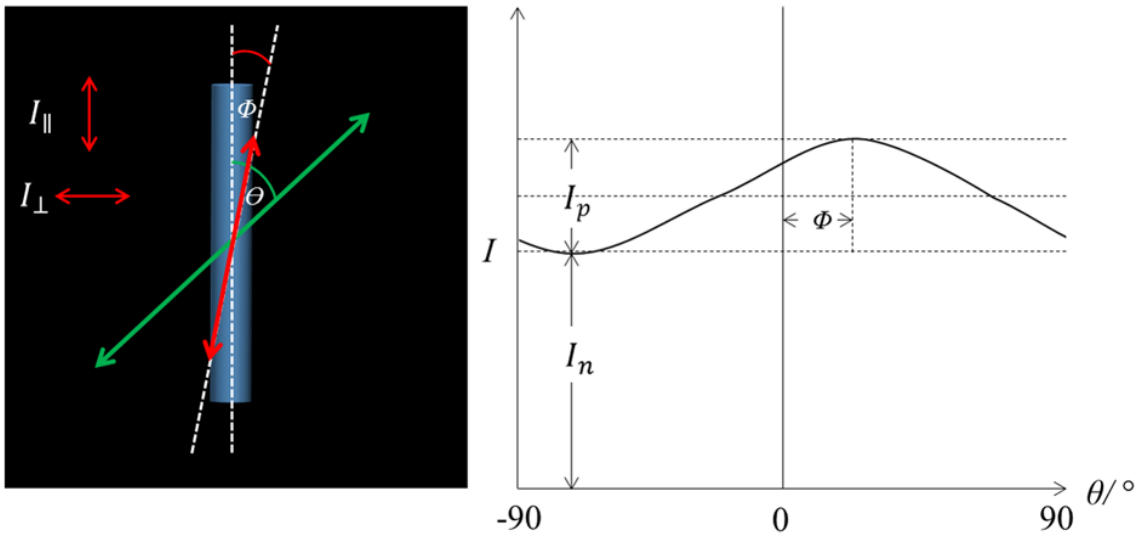

Figure A.1 Overview of polarization measurements and interpretation.

APPENDIX B

OPTIMIZED COORDINATES FOR THE OPTIMIZED HOST-GUEST COMPLEX

optimized (PBEsol-D3/DZP) coordinates (in Å) for the optimized host-guest complex model corresponding to Figure 3.11. Host atom positions are derived from CIF file describing **1** crystallized from nitrobenzene as published in Ref. 1.

Table B.1 Optimized (PBEsol-D3/DZP) coordinates (in Å) for the optimized host-guest complex model corresponding to Figure 3.11.

Atom	x	y	z
C	2.890624	-5.33478	5.790823
C	0.576812	-5.29449	6.621409
H	0.646998	-5.58634	7.565312
H	0.41675	-6.09461	6.061508
C	-0.57245	-4.3234	6.469813
C	-1.23982	-3.83293	7.572299
H	-0.99405	-4.13368	8.440252
C	-2.26533	-2.90587	7.436805
H	-2.70837	-2.57327	8.209365
C	-2.64514	-2.46412	6.175736
C	-1.99303	-2.97332	5.054415
H	-2.25122	-2.68944	4.184031
C	-0.97031	-3.89149	5.206618
H	-0.53027	-4.23392	4.436184
C	-3.70286	-1.4949	6.006824
C	-4.56351	-0.69244	5.839431

C	-5.57483	0.302547	5.569354
C	-6.43675	0.746637	6.576143
H	-6.37486	0.380778	7.449868
C	-7.38513	1.725698	6.29604
H	-7.97301	2.024101	6.97898
C	-7.47715	2.266289	5.027377
H	-8.12252	2.93992	4.846312
C	-6.62904	1.827352	4.016638
C	-5.68096	0.844543	4.288538
H	-5.10283	0.541456	3.597699
C	-6.7132	2.387618	2.687822
C	-6.75694	2.815781	1.562247
C	-6.82243	3.223801	0.193026
C	-7.99891	3.296879	-0.5127
H	-8.82033	3.132453	-0.06308
C	-8.01821	3.604182	-1.85853
H	-8.84934	3.610272	-2.31726
C	-6.89877	3.893684	-2.53691
C	-5.62877	3.837939	-1.86157
H	-4.82154	3.997212	-2.33549
C	-5.60714	3.5475	-0.50966
H	-4.78087	3.561553	-0.03877
C	-6.90651	4.20333	-4.01337
H	-7.72966	3.82857	-4.41348
H	-6.9327	5.18567	-4.13398
N	3.975833	-4.57261	5.470011
H	3.864155	-3.70926	5.535936

N	1.816448	-4.64475	6.211584
H	1.8666	-3.76547	6.255939
O	2.905279	-6.57898	5.727633
C	-4.67258	4.437087	-5.04204
C	-2.35877	4.3968	-5.87262
H	-2.42896	4.688644	-6.81652
H	-2.19871	5.196912	-5.31272
C	-1.20951	3.425703	-5.72103
C	-0.54214	2.935236	-6.82351
H	-0.78791	3.235981	-7.69146
C	0.483366	2.008173	-6.68802
H	0.926413	1.675574	-7.46058
C	0.863182	1.566425	-5.42695
C	0.211065	2.07563	-4.30563
H	0.469255	1.791749	-3.43524
C	-0.81165	2.993792	-4.45783
H	-1.25169	3.336229	-3.6874
C	1.920897	0.597202	-5.25804
C	2.781547	-0.20525	-5.09064
C	3.792873	-1.20024	-4.82057
C	4.654788	-1.64433	-5.82736
H	4.592902	-1.27847	-6.70108
C	5.603167	-2.62339	-5.54725
H	6.191046	-2.9218	-6.23019
C	5.695186	-3.16398	-4.27859
H	6.340557	-3.83761	-4.09752
C	4.847077	-2.72505	-3.26785

C	3.898997	-1.74224	-3.53975
H	3.320868	-1.43915	-2.84891
C	4.931241	-3.28531	-1.93903
C	4.974984	-3.71348	-0.81346
C	5.040473	-4.1215	0.555762
C	6.216954	-4.19457	1.261487
H	7.038365	-4.03015	0.811864
C	6.236245	-4.50188	2.607315
H	7.067379	-4.50797	3.066051
C	5.116812	-4.79138	3.285698
C	3.846814	-4.73563	2.610353
H	3.039579	-4.89491	3.084279
C	3.825175	-4.44519	1.258449
H	2.998914	-4.45925	0.78756
C	5.124546	-5.10102	4.76216
H	5.947695	-4.72626	5.162263
H	5.150738	-6.08336	4.882768
N	-5.75779	3.674918	-4.72122
H	-5.64612	2.811565	-4.78715
N	-3.59841	3.74706	-5.4628
H	-3.64856	2.867779	-5.50715
O	-4.68724	5.68129	-4.97885
C	2.890624	-0.65028	5.790823
C	0.576812	-0.60999	6.621409
H	0.646998	-0.90184	7.565312
H	0.41675	-1.41011	6.061508
C	-0.57245	0.361103	6.469813

C	-1.23982	0.85157	7.572299
H	-0.99405	0.550825	8.440252
C	-2.26533	1.778633	7.436805
H	-2.70837	2.111232	8.209365
C	-2.64514	2.220381	6.175736
C	-1.99303	1.711176	5.054415
H	-2.25122	1.995057	4.184031
C	-0.97031	0.793014	5.206618
H	-0.53027	0.450577	4.436184
C	-3.70286	3.189604	6.006824
C	-4.56351	3.992059	5.839431
C	-5.57483	4.987047	5.569354
C	-6.43675	5.431137	6.576143
H	-6.37486	5.065278	7.449868
C	-7.38513	6.410198	6.29604
H	-7.97301	6.708601	6.97898
C	-7.47715	6.950789	5.027377
H	-8.12252	7.62442	4.846312
C	-6.62904	6.511852	4.016638
C	-5.68096	5.529043	4.288538
H	-5.10283	5.225956	3.597699
C	-6.7132	7.072118	2.687822
C	-6.75694	7.500281	1.562247
C	-6.82243	7.908301	0.193026
C	-7.99891	7.981379	-0.5127
H	-8.82033	7.816953	-0.06308
C	-8.01821	8.288682	-1.85853

H	-8.84934	8.294772	-2.31726
C	-6.89877	8.578184	-2.53691
C	-5.62877	8.522439	-1.86157
H	-4.82154	8.681712	-2.33549
C	-5.60714	8.232	-0.50966
H	-4.78087	8.246053	-0.03877
C	-6.90651	8.88783	-4.01337
H	-7.72966	8.51307	-4.41348
H	-6.9327	9.87017	-4.13398
N	3.975833	0.111888	5.470011
H	3.864155	0.975241	5.535936
N	1.816448	0.039746	6.211584
H	1.8666	0.919027	6.255939
O	2.905279	-1.89448	5.727633
C	-4.67258	9.121587	-5.04204
C	-2.35877	9.0813	-5.87262
H	-2.42896	9.373144	-6.81652
H	-2.19871	9.881412	-5.31272
C	-1.20951	8.110203	-5.72103
C	-0.54214	7.619736	-6.82351
H	-0.78791	7.920481	-7.69146
C	0.483366	6.692673	-6.68802
H	0.926413	6.360074	-7.46058
C	0.863182	6.250925	-5.42695
C	0.211065	6.76013	-4.30563
H	0.469255	6.476249	-3.43524
C	-0.81165	7.678292	-4.45783

H	-1.25169	8.020729	-3.6874
C	1.920897	5.281702	-5.25804
C	2.781547	4.479247	-5.09064
C	3.792873	3.484259	-4.82057
C	4.654788	3.040169	-5.82736
H	4.592902	3.406028	-6.70108
C	5.603167	2.061108	-5.54725
H	6.191046	1.762705	-6.23019
C	5.695186	1.520517	-4.27859
H	6.340557	0.846886	-4.09752
C	4.847077	1.959454	-3.26785
C	3.898997	2.942263	-3.53975
H	3.320868	3.24535	-2.84891
C	4.931241	1.399188	-1.93903
C	4.974984	0.971025	-0.81346
C	5.040473	0.563005	0.555762
C	6.216954	0.489927	1.261487
H	7.038365	0.654353	0.811864
C	6.236245	0.182624	2.607315
H	7.067379	0.176534	3.066051
C	5.116812	-0.10688	3.285698
C	3.846814	-0.05113	2.610353
H	3.039579	-0.21041	3.084279
C	3.825175	0.239306	1.258449
H	2.998914	0.225253	0.78756
C	5.124546	-0.41652	4.76216
H	5.947695	-0.04176	5.162263

H	5.150738	-1.39886	4.882768
N	-5.75779	8.359418	-4.72122
H	-5.64612	7.496065	-4.78715
N	-3.59841	8.43156	-5.4628
H	-3.64856	7.552279	-5.50715
O	-4.68724	10.36579	-4.97885
C	2.890624	4.034219	5.790823
C	0.576812	4.074506	6.621409
H	0.646998	3.782662	7.565312
H	0.41675	3.274394	6.061508
C	-0.57245	5.045603	6.469813
C	-1.23982	5.53607	7.572299
H	-0.99405	5.235325	8.440252
C	-2.26533	6.463133	7.436805
H	-2.70837	6.795732	8.209365
C	-2.64514	6.904881	6.175736
C	-1.99303	6.395676	5.054415
H	-2.25122	6.679557	4.184031
C	-0.97031	5.477514	5.206618
H	-0.53027	5.135077	4.436184
C	-3.70286	7.874104	6.006824
C	-4.56351	8.676559	5.839431
C	-5.57483	9.671547	5.569354
C	-6.43675	10.11564	6.576143
H	-6.37486	9.749778	7.449868
C	-7.38513	11.0947	6.29604
H	-7.97301	11.3931	6.97898

C	-7.47715	11.63529	5.027377
H	-8.12252	12.30892	4.846312
C	-6.62904	11.19635	4.016638
C	-5.68096	10.21354	4.288538
H	-5.10283	9.910456	3.597699
C	-6.7132	11.75662	2.687822
C	-6.75694	12.18478	1.562247
C	-6.82243	12.5928	0.193026
C	-7.99891	12.66588	-0.5127
H	-8.82033	12.50145	-0.06308
C	-8.01821	12.97318	-1.85853
H	-8.84934	12.97927	-2.31726
C	-6.89877	13.26269	-2.53691
C	-5.62877	13.20694	-1.86157
H	-4.82154	13.36621	-2.33549
C	-5.60714	12.9165	-0.50966
H	-4.78087	12.93055	-0.03877
C	-6.90651	13.57233	-4.01337
H	-7.72966	13.19757	-4.41348
H	-6.9327	14.55467	-4.13398
N	3.975833	4.796388	5.470011
H	3.864155	5.659741	5.535936
N	1.816448	4.724246	6.211584
H	1.8666	5.603527	6.255939
O	2.905279	2.790016	5.727633
C	-4.67258	13.80609	-5.04204
C	-2.35877	13.7658	-5.87262

H	-2.42896	14.05764	-6.81652
H	-2.19871	14.56591	-5.31272
C	-1.20951	12.7947	-5.72103
C	-0.54214	12.30424	-6.82351
H	-0.78791	12.60498	-7.69146
C	0.483366	11.37717	-6.68802
H	0.926413	11.04457	-7.46058
C	0.863182	10.93543	-5.42695
C	0.211065	11.44463	-4.30563
H	0.469255	11.16075	-3.43524
C	-0.81165	12.36279	-4.45783
H	-1.25169	12.70523	-3.6874
C	1.920897	9.966202	-5.25804
C	2.781547	9.163747	-5.09064
C	3.792873	8.168759	-4.82057
C	4.654788	7.724669	-5.82736
H	4.592902	8.090528	-6.70108
C	5.603167	6.745608	-5.54725
H	6.191046	6.447205	-6.23019
C	5.695186	6.205017	-4.27859
H	6.340557	5.531386	-4.09752
C	4.847077	6.643954	-3.26785
C	3.898997	7.626763	-3.53975
H	3.320868	7.92985	-2.84891
C	4.931241	6.083688	-1.93903
C	4.974984	5.655525	-0.81346
C	5.040473	5.247505	0.555762

C	6.216954	5.174427	1.261487
H	7.038365	5.338853	0.811864
C	6.236245	4.867124	2.607315
H	7.067379	4.861034	3.066051
C	5.116812	4.577622	3.285698
C	3.846814	4.633367	2.610353
H	3.039579	4.474094	3.084279
C	3.825175	4.923806	1.258449
H	2.998914	4.909753	0.78756
C	5.124546	4.267976	4.76216
H	5.947695	4.642736	5.162263
H	5.150738	3.285636	4.882768
N	-5.75779	13.04392	-4.72122
H	-5.64612	12.18057	-4.78715
N	-3.59841	13.11606	-5.4628
H	-3.64856	12.23678	-5.50715
O	-4.68724	15.05029	-4.97885
C	2.890624	8.718719	5.790823
C	0.576812	8.759006	6.621409
H	0.646998	8.467162	7.565312
H	0.41675	7.958894	6.061508
C	-0.57245	9.730103	6.469813
C	-1.23982	10.22057	7.572299
H	-0.99405	9.919825	8.440252
C	-2.26533	11.14763	7.436805
H	-2.70837	11.48023	8.209365
C	-2.64514	11.58938	6.175736

C	-1.99303	11.08018	5.054415
H	-2.25122	11.36406	4.184031
C	-0.97031	10.16201	5.206618
H	-0.53027	9.819577	4.436184
C	-3.70286	12.5586	6.006824
C	-4.56351	13.36106	5.839431
C	-5.57483	14.35605	5.569354
C	-6.43675	14.80014	6.576143
H	-6.37486	14.43428	7.449868
C	-7.38513	15.7792	6.29604
H	-7.97301	16.0776	6.97898
C	-7.47715	16.31979	5.027377
H	-8.12252	16.99342	4.846312
C	-6.62904	15.88085	4.016638
C	-5.68096	14.89804	4.288538
H	-5.10283	14.59496	3.597699
C	-6.7132	16.44112	2.687822
C	-6.75694	16.86928	1.562247
C	-6.82243	17.2773	0.193026
C	-7.99891	17.35038	-0.5127
H	-8.82033	17.18595	-0.06308
C	-8.01821	17.65768	-1.85853
H	-8.84934	17.66377	-2.31726
C	-6.89877	17.94718	-2.53691
C	-5.62877	17.89144	-1.86157
H	-4.82154	18.05071	-2.33549
C	-5.60714	17.601	-0.50966

H	-4.78087	17.61505	-0.03877
C	-6.90651	18.25683	-4.01337
H	-7.72966	17.88207	-4.41348
H	-6.9327	19.23917	-4.13398
N	3.975833	9.480888	5.470011
H	3.864155	10.34424	5.535936
N	1.816448	9.408746	6.211584
H	1.8666	10.28803	6.255939
O	2.905279	7.474516	5.727633
C	-4.67258	18.49059	-5.04204
C	-2.35877	18.4503	-5.87262
H	-2.42896	18.74214	-6.81652
H	-2.19871	19.25041	-5.31272
C	-1.20951	17.4792	-5.72103
C	-0.54214	16.98874	-6.82351
H	-0.78791	17.28948	-7.69146
C	0.483366	16.06167	-6.68802
H	0.926413	15.72907	-7.46058
C	0.863182	15.61993	-5.42695
C	0.211065	16.12913	-4.30563
H	0.469255	15.84525	-3.43524
C	-0.81165	17.04729	-4.45783
H	-1.25169	17.38973	-3.6874
C	1.920897	14.6507	-5.25804
C	2.781547	13.84825	-5.09064
C	3.792873	12.85326	-4.82057
C	4.654788	12.40917	-5.82736

H	4.592902	12.77503	-6.70108
C	5.603167	11.43011	-5.54725
H	6.191046	11.13171	-6.23019
C	5.695186	10.88952	-4.27859
H	6.340557	10.21589	-4.09752
C	4.847077	11.32845	-3.26785
C	3.898997	12.31126	-3.53975
H	3.320868	12.61435	-2.84891
C	4.931241	10.76819	-1.93903
C	4.974984	10.34003	-0.81346
C	5.040473	9.932005	0.555762
C	6.216954	9.858927	1.261487
H	7.038365	10.02335	0.811864
C	6.236245	9.551624	2.607315
H	7.067379	9.545534	3.066051
C	5.116812	9.262121	3.285698
C	3.846814	9.317867	2.610353
H	3.039579	9.158594	3.084279
C	3.825175	9.608306	1.258449
H	2.998914	9.594253	0.78756
C	5.124546	8.952476	4.76216
H	5.947695	9.327236	5.162263
H	5.150738	7.970136	4.882768
N	-5.75779	17.72842	-4.72122
H	-5.64612	16.86507	-4.78715
N	-3.59841	17.80056	-5.4628
H	-3.64856	16.92128	-5.50715

O	-4.68724	19.73479	-4.97885
C	2.890624	13.40322	5.790823
C	0.576812	13.44351	6.621409
H	0.646998	13.15166	7.565312
H	0.41675	12.64339	6.061508
C	-0.57245	14.4146	6.469813
C	-1.23982	14.90507	7.572299
H	-0.99405	14.60433	8.440252
C	-2.26533	15.83213	7.436805
H	-2.70837	16.16473	8.209365
C	-2.64514	16.27388	6.175736
C	-1.99303	15.76468	5.054415
H	-2.25122	16.04856	4.184031
C	-0.97031	14.84651	5.206618
H	-0.53027	14.50408	4.436184
C	-3.70286	17.2431	6.006824
C	-4.56351	18.04556	5.839431
C	-5.57483	19.04055	5.569354
C	-6.43675	19.48464	6.576143
H	-6.37486	19.11878	7.449868
C	-7.38513	20.4637	6.29604
H	-7.97301	20.7621	6.97898
C	-7.47715	21.00429	5.027377
H	-8.12252	21.67792	4.846312
C	-6.62904	20.56535	4.016638
C	-5.68096	19.58254	4.288538
H	-5.10283	19.27946	3.597699

C	-6.7132	21.12562	2.687822
C	-6.75694	21.55378	1.562247
C	-6.82243	21.9618	0.193026
C	-7.99891	22.03488	-0.5127
H	-8.82033	21.87045	-0.06308
C	-8.01821	22.34218	-1.85853
H	-8.84934	22.34827	-2.31726
C	-6.89877	22.63168	-2.53691
C	-5.62877	22.57594	-1.86157
H	-4.82154	22.73521	-2.33549
C	-5.60714	22.2855	-0.50966
H	-4.78087	22.29955	-0.03877
C	-6.90651	22.94133	-4.01337
H	-7.72966	22.56657	-4.41348
H	-6.9327	23.92367	-4.13398
N	3.975833	14.16539	5.470011
H	3.864155	15.02874	5.535936
N	1.816448	14.09325	6.211584
H	1.8666	14.97253	6.255939
O	2.905279	12.15902	5.727633
C	-4.67258	23.17509	-5.04204
C	-2.35877	23.1348	-5.87262
H	-2.42896	23.42664	-6.81652
H	-2.19871	23.93491	-5.31272
C	-1.20951	22.1637	-5.72103
C	-0.54214	21.67324	-6.82351
H	-0.78791	21.97398	-7.69146

C	0.483366	20.74617	-6.68802
H	0.926413	20.41357	-7.46058
C	0.863182	20.30443	-5.42695
C	0.211065	20.81363	-4.30563
H	0.469255	20.52975	-3.43524
C	-0.81165	21.73179	-4.45783
H	-1.25169	22.07423	-3.6874
C	1.920897	19.3352	-5.25804
C	2.781547	18.53275	-5.09064
C	3.792873	17.53776	-4.82057
C	4.654788	17.09367	-5.82736
H	4.592902	17.45953	-6.70108
C	5.603167	16.11461	-5.54725
H	6.191046	15.81621	-6.23019
C	5.695186	15.57402	-4.27859
H	6.340557	14.90039	-4.09752
C	4.847077	16.01295	-3.26785
C	3.898997	16.99576	-3.53975
H	3.320868	17.29885	-2.84891
C	4.931241	15.45269	-1.93903
C	4.974984	15.02453	-0.81346
C	5.040473	14.61651	0.555762
C	6.216954	14.54343	1.261487
H	7.038365	14.70785	0.811864
C	6.236245	14.23612	2.607315
H	7.067379	14.23003	3.066051
C	5.116812	13.94662	3.285698

C	3.846814	14.00237	2.610353
H	3.039579	13.84309	3.084279
C	3.825175	14.29281	1.258449
H	2.998914	14.27875	0.78756
C	5.124546	13.63698	4.76216
H	5.947695	14.01174	5.162263
H	5.150738	12.65464	4.882768
N	-5.75779	22.41292	-4.72122
H	-5.64612	21.54957	-4.78715
N	-3.59841	22.48506	-5.4628
H	-3.64856	21.60578	-5.50715
O	-4.68724	24.41929	-4.97885
S	-2.61781	8.168982	1.354661
C	-2.40717	9.514235	0.245935
C	-2.5102	7.017255	0.042198
C	-2.25731	7.657936	-1.1664
C	-2.19092	9.052115	-1.0398
H	-2.07767	9.735152	-1.88754
H	-2.21201	7.125676	-2.11572
C	-2.45313	10.85629	0.737693
S	-1.41014	12.08654	0.074689
C	-3.25817	11.37011	1.747864
C	-2.10565	13.26065	1.14303
C	-3.06647	12.73534	1.978575
H	-4.01997	10.76844	2.244662
H	-3.60902	13.34394	2.701402
N	-2.64126	5.680211	0.264719

C	-2.84594	5.231356	1.618917
C	-1.95887	4.801773	-0.67122
H	-0.87856	5.04214	-0.73474
H	-2.40203	4.889194	-1.6765
H	-2.07662	3.762811	-0.32954
H	-3.69938	5.788503	2.050216
H	-3.10604	4.160073	1.624187
H	-1.95201	5.385125	2.262764
N	-1.6613	14.6003	1.097782
O	-0.75735	14.87464	0.293427
O	-2.20162	15.40511	1.865582

APPENDIX C

COPYRIGHT PERMISSION

11/2/2017 Rightslink® by Copyright Clearance Center

Copyright Clearance Center RightsLink®

Home | Create Account | Help

ACS Publications Most Trusted. Most Cited. Most Read.

Title: Fluorescence Polarization Measurements to Probe Alignment of a Bithiophene Dye in One-Dimensional Channels of Self-Assembled Phenylethynylene Bis-Urea Macrocycle Crystals

Author: Preecha Kittikhunnatham, Bozumeh Som, Vitaly Rassolov, et al

Publication: The Journal of Physical Chemistry C

Publisher: American Chemical Society

Date: Aug 1, 2017

Copyright © 2017, American Chemical Society

LOGIN

If you're a copyright.com user, you can login to RightsLink using your copyright.com credentials. Already a RightsLink user or want to learn more?

PERMISSION/LICENSE IS GRANTED FOR YOUR ORDER AT NO CHARGE

This type of permission/license, instead of the standard Terms & Conditions, is sent to you because no fee is being charged for your order. Please note the following:

- Permission is granted for your request in both print and electronic formats, and translations.
- If figures and/or tables were requested, they may be adapted or used in part.
- Please print this page for your records and send a copy of it to your publisher/graduate school.
- Appropriate credit for the requested material should be given as follows: "Reprinted (adapted) with permission from (COMPLETE REFERENCE CITATION). Copyright (YEAR) American Chemical Society." Insert appropriate information in place of the capitalized words.
- One-time permission is granted only for the use specified in your request. No additional uses are granted (such as derivative works or other editions). For any other uses, please submit a new request.

BACK | CLOSE WINDOW

Copyright © 2017 Copyright Clearance Center, Inc. All Rights Reserved. Privacy statement. Terms and Conditions.
Comments? We would like to hear from you. E-mail us at customercare@copyright.com